Hyperglycemic environments directly compromise intestinal epithelial barrier function in an organoid model and hyaluronan (~35kDa) protects via a layilin dependent mechanism

Samreen Jatana , Amina Abbadi , Gail A. West , András K. Ponti , Manuel B. Braga-Neto , Jordyn L. Smith , Armando Marino-Melendez , Belinda Willard , Laura E. Nagy , Carol de la Motte

PII: S0945-053X(24)00109-4
DOI: https://doi.org/10.1016/j.matbio.2024.08.007
Reference: MATBIO 1901

To appear in: *Matrix Biology*

Received date: 1 May 2024
Revised date: 12 August 2024
Accepted date: 23 August 2024

Please cite this article as: Samreen Jatana , Amina Abbadi , Gail A. West , András K. Ponti , Manuel B. Braga-Neto , Jordyn L. Smith , Armando Marino-Melendez , Belinda Willard , Laura E. Nagy , Carol de la Motte , Hyperglycemic environments directly compromise intestinal epithelial barrier function in an organoid model and hyaluronan (~35kDa) protects via a layilin dependent mechanism, *Matrix Biology* (2024), doi: https://doi.org/10.1016/j.matbio.2024.08.007

Highlights

- Hyperglycemic stress increases protein loss and spatial distribution of key intestinal barrier proteins in a mouse intestinal organoid model.
- Small molecular weight hyaluronan (35 kDa), HA35, plays a protective effect on barrier function under high glucose conditions.
- HA35 regulates apoptotic cell death in organoids grown under hyperglycemic stress.
- The effects of HA35 on the intestinal barrier function are likely regulated by its receptor layilin via the layilin-integrin-FAK axis.

Hyperglycemic environments directly compromise intestinal epithelial barrier function in an organoid model and hyaluronan (~35kDa) protects via a layilin dependent mechanism

Samreen Jatana[1], Amina Abbadi[1], Gail A. West[1], András K. Ponti[2], Manuel B. Braga-Neto[3], Jordyn L. Smith[1], Armando Marino-Melendez[1], Belinda Willard[4], Laura E. Nagy[1,5,6,7], Carol de la Motte[1,6]

1 Department of Inflammation & Immunity, Lerner Research Institute, Cleveland Clinic, Cleveland, Ohio, United States

2 Department of Cardiovascular & Metabolic Sciences, Lerner Research Institute, Cleveland Clinic, Cleveland, Ohio, United States

3 Department of Gastroenterology, Hepatology and Nutrition, Digestive Diseases and Surgery Institute, Cleveland Clinic Foundation, Cleveland, Ohio, United States

4 Proteomics and Metabolomics Core, Lerner Research Institute, Cleveland Clinic, Cleveland, Ohio, United States

5 Northern Ohio Alcohol Center, Department of Inflammation and Immunity, Cleveland Clinic, Cleveland, Ohio, United States

6 Department of Gastroenterology and Hepatology, Cleveland Clinic, Cleveland, Ohio, United States

7 Department of Molecular Medicine, Cleveland Clinic Lerner College of Medicine, Case Western Reserve University, Cleveland, Ohio, United States

Abstract

Background: Metabolic syndrome and diabetes in obese individuals are strong risk factors for development of inflammatory bowel disease (IBD) and colorectal cancer. The pathogenic mechanisms of low-grade metabolic inflammation, including chronic hyperglycemic stress, in disrupting gut homeostasis are poorly understood. In this study, we sought to understand the impact of a hyperglycemic environment on intestinal barrier integrity and the protective effects of small molecular weight (35 kDa) hyaluronan on epithelial barrier function.

Methods: Intestinal organoids derived from mouse colon were grown in normal glucose media (5 mM) or high glucose media (25 mM) to study the impact of hyperglycemic stress on the intestinal barrier. Additionally, organoids were pretreated with 35 kDa hyaluronan (HA35) to investigate the effect of hyaluronan on epithelial barrier under high glucose stress. Immunoblotting as well as confocal imaging was used to understand changes in barrier proteins, quantitative as well as spatial distribution, respectively. Alterations in barrier function were measured using trans-epithelial electrical resistance and fluorescein isothiocyanate flux assays. Untargeted proteomics analysis was performed to elucidate mechanisms by which HA35 exerts a protective effect on the barrier. Intestinal organoids derived from receptor knockout mice specific to various HA receptors were utilized to understand the role of HA receptors in barrier protection under high glucose conditions.

Results: We found that high glucose stress decreased the protein expression as well as spatial distribution of two key barrier proteins, zona occludens-1 (ZO-1) and occludin. HA35 prevented the degradation or loss of ZO-1 and maintained the spatial distribution of both ZO-1 and occludin under hyperglycemic stress. Functionally, we also observed a protective effect of HA35 on the epithelial barrier under high glucose conditions. We found that HA receptor, layilin, was involved in preventing barrier protein loss (ZO-1) as well as maintaining spatial distribution of ZO-1 and occludin. Additionally, proteomics analysis showed that cell death and survival was the primary pathway upregulated in organoids treated with HA35 under high glucose stress. We found that XIAP associated factor 1 (Xaf1) was modulated by HA35 thereby regulating apoptotic cell death in the intestinal organoid system. Finally, we observed that spatial organization of both focal adhesion kinase (FAK) as well as F-actin was mediated by HA35 via layilin.

Conclusion: Our results highlight the impact of hyperglycemic stress on the intestinal barrier function. This is of clinical relevance, as impaired barrier function has been observed in individuals

with metabolic syndrome. Additionally, we demonstrate barrier protective effects of HA35 through its receptor layilin and modulation of cellular apoptosis under high glucose stress.

Keywords

Hyperglycemia, metabolic syndrome, hyaluronan, intestinal barrier, organoids, apoptosis, layilin.

Abbreviations

High density lipids (HDL), Inflammatory bowel disease (IBD), Type 2 diabetes (T2D), Extracellular matrix (ECM), Hyaluronan (HA), 35 kDa Hyaluronan (HA35), Zona occludens-1 (ZO-1), Toll-like receptor 2 (TLR2), Toll-like receptor 4 (TLR4), XIAP associated factor 1 (XAF1), Trans-epithelial electrical resistance (TEER), Fluorescein isothiocyanate (FITC), Focal adhesion kinase (FAK).

Introduction

Hyperglycemia is a condition of growing health concern that is strongly linked to chronic diseases such as obesity and metabolic syndrome, and high glucose stress is a key factor that contributes to the underlying low grade chronic metabolic inflammation, termed metaflammation [1, 2]. A recent study showed that in the year 2022, approximately 1 billion people in the world were living with obesity, including children and adolescents [3]. Increased blood glucose, triglycerides, and high-density lipid (HDL) cholesterol are among the hallmarks of metabolic disease [4]. Emerging research also suggests that metabolic syndrome and diabetes in obese individuals are strong risk factors for the development of inflammatory bowel disease (IBD) as well as colorectal cancer [5-13]. While the contribution of metabolic tissues such as adipose, pancreas, and liver has been widely studied in metabolic disease pathogenesis, there is growing appreciation that the intestine might also play a role in metabolic dysfunction. How glucose stress-mediated intestinal perturbations may contribute to metaflammation is poorly understood.

The intestinal barrier plays a homeostatic as well as a protective role in the body. This protective barrier function is partially mediated by the action of tight junctions (comprised of claudins, occludin, zona occludens proteins) that are apically located in polarized epithelial cells along with adherens junctions [14, 15]. Dietary intake, alterations in the gut microbiome, and pro-inflammatory stimuli can induce structural as well as functional changes in the barrier [16]. Glucotoxicity, lipotoxicity and pro-inflammatory mediators that constitute a metabolic stress environment can cause intestinal barrier impairment and make it “leakier”. Specifically, recent clinical studies have shown that poor glycemic control can lead to gut barrier impairment in chronic disease conditions like type 2 diabetes (T2D) [17-19]. A clinical study that investigated alterations in the intestinal barrier in chronic T2D patients found elevated levels of serum lipopolysaccharide (LPS), and zonulin indicative of impaired barrier function [20]. Similarly, using well-established animal models of obesity and diabetes, Thaiss et al. demonstrated that hyperglycemia increased the risk of systemic infection in obese mice with altered tight junctions and adherens junctions [21]. While studies have begun to explore the mechanistic basis of barrier dysfunction in obesity [21, 22], there is a still a huge gap in knowledge in terms of identifying how individual pro-inflammatory stress signals such as hyperglycemia impact intestinal disease pathogenesis.

Previous studies in our group have focused on understanding the role of hyaluronan (HA), an abundant extracellular matrix (ECM) constituent in the body, in innate host defense mechanisms in the gut [23]. HA is an abundant glycosaminoglycan present in the extracellular matrix of the intestine. HA is a polymer that is synthesized on cell surfaces by HA synthase

enzymes and is comprised of repeating disaccharide units of N-acetylglucosamine and glucuronic acid [24]. During tissue injury or inflammation such as IBD, high molecular weight HA can be degraded by hyaluronidases into smaller fragments that can act as damage-associated molecular patterns (DAMPs) [23]. These smaller HA fragments in the ECM can signal via known HA receptors present on neighboring cells including CD44, toll-like receptor (TLR) 2/4, and layilin [13]. Therefore, in addition to providing structural support as an ECM component, HA can also act as a signaling moiety based on fragment size [13, 24]. Our group has studied the role of HA in innate defense mechanisms in IBD as well as intestinal infection models [23, 25-28]. In the context of intestinal barrier function, we have previously shown that specific-sized 35 kDa molecular weight HA (HA35) protected mice from necrotizing enterocolitis and Citrobacter infection by upregulating zona occludens (ZO)-1 expression in the gut thereby enhancing epithelial barrier function [26, 29]. A similar barrier protective effect of HA35 was observed in an animal model of colitis [27]. Additionally, we have reported that HA35 treatment increased ZO-1 expression in mouse intestinal organoids [27]. Using *in vitro* intestinal mouse organoids, we showed that layilin but not CD44 or TLR4 was involved in the barrier protective effect of HA35 [27]. In addition to studying the role of HA as a major constituent of the ECM, we have also explored how oral administration of HA could provide beneficial effects in the gut. We found that oral administration of human milk-derived HA in wild-type mice resulted in increased production of murine beta defensin 2 and protected the mice from Salmonella infection [30]. HA35 was also found to play a protective role in maintaining barrier integrity in various models of ethanol-induced intestinal barrier disruption [31, 32]. More recently, we tested the safety and tolerability of HA35 in human subjects and found that oral administration of pharmaceutical grade HA35 was well tolerated in humans with no adverse effects or changes as measured through clinical, biochemical tests as well as microbiome composition in the stool [33].

In the current study, we hypothesized that HA35 would play a barrier protective role in the colon under high glycemic exposure, a condition pertinent to Western diet in general, as well as being a specific contributor to a pro-inflammatory milieu in diabetic individuals. Our experiments employed an *in vitro* organoid system. Intestinal organoids permit investigation of strictly epithelial cell mechanisms in a sterile environment not influenced by the many additional stimuli provided by the *in vivo* intestinal microenvironment such as such as inflammatory cytokines, hormones, immune cells, and microbial stimuli. This system more accurately recapitulates the complex biology of normal intestinal epithelium in comparison to cancer associated, immortalized intestinal cell lines, that were for many years the only models available. Additionally, in our study we were also able to evaluate the role of an epithelial barrier promoting molecule, specific-sized HA35, in

combination with high glucose as a complimentary biologic factor. Of note, crypt base stem cells isolated from mouse distal colon tissue were grown and expanded in normal glucose media (5 mM, 1 g/L). Under test conditions, high glucose (25 mM, 4.5 g/L) was added to the test cultures to simulate a hyperglycemic stress environment comparable to systemic blood glucose measured in diabetic individuals, yet likely not as severe as could be achieved at times in the GI tract with a sugar rich diet. Results obtained from the study showed that HA35 plays a barrier protective role in a high glucose environment by preventing the protein loss and preserving the spatial distribution of a key barrier protein, ZO-1. HA35 also maintained the spatial distribution of occludin under high glucose stress. Proteomics analysis revealed that cell death and survival was the top cellular process pathway upregulated in organoids treated with HA35 under high glucose conditions. XIAP Associated Factor 1 (Xaf1), a key protein involved in apoptotic cell death, was downregulated under high glycemic exposure. We demonstrated that HA35 treatment increased cellular Xaf1 expression under high glucose conditions and maintained cellular apoptosis as well as proliferation at near baseline (normal glucose controls), which maybe a key to maintaining a healthy barrier. Finally, we demonstrated that the HA receptor, layilin, was important in mediating the protective effect of HA35 under high glucose conditions.

Results

HA35 protects against the effects of hyperglycemia on tight junction protein expression

To elucidate the effect of a high glucose environment on the intestinal epithelial barrier, we evaluated the protein and gene expression of tight junction proteins in intestinal organoids derived from colonic crypt base stem cells from genetically wild type (C57BL/6J) mice. Organoids were cultured [34], and expanded under “normal glucose” (5 mM, 1 g/L) conditions. Test conditions employed the same culture medium with “high glucose” (25 mM, 4.5 g/L). Normal and high glucose conditions used reflect the clinical fasting blood glucose concentration in healthy (<100 mg/dl) and diabetic patients (>126 mg/dl), respectively. In experiments, cultured organoids were treated for 30-48 hours in high glucose (25 mM) and normal glucose (5 mM) conditions (**Fig. 1A**), except when noted in time course studies. Importantly, to determine whether HA35 had protective effects on tight junction proteins, replicate organoid cultures were pre-treated with HA35, 24 hours prior to culturing them in high glucose (**Fig. 1A**). Tight junction proteins including ZO-1, occludin and claudin-1 in organoid cell extracts were quantified using western blot analysis. Intestinal organoids cultured in high glucose medium had lower protein expression of the junctional proteins ZO-1 and occludin compared to the normoglycemic cultured controls (**Fig. 1B, C**). No changes were observed in claudin-1 protein under hyperglycemic stress in comparison to normal glucose

controls (**Fig. 1D**). HA35 pre-treatment dampened the downregulation of tight junction protein expression of ZO-1, but not occludin and claudin-1, in organoids exposed to high glucose, yet had little effect in normal glucose cultures (**Fig. 1B-D**). Importantly, the relative gene expression of tight junction proteins including ZO-1, occludin, and claudin-1 was maintained at near baseline expression and unaffected by the high concentration of glucose and/or HA35 throughout an extended time course. (**Supplemental Fig. 1**). Together these data suggest that downregulation of ZO-1 protein expression in intestinal organoids under hyperglycemic stress likely causes protein loss or degradation, which HA35 largely prevents.

HA35 pre-treatment maintains spatial distribution of ZO-1 and occludin under high glucose conditions

Since high glucose concentration appears to increase loss or degradation of ZO-1 protein, we questioned whether hyperglycemic stress alters the spatial arrangement of tight junction proteins within organoids and whether HA35 pre-treatment maintains their cellular localization. Employing the same treatment protocol as above (**Fig. 1A**), we analyzed the spatial distribution of tight junction proteins in whole mount formalin-fixed intestinal organoids using fluorescence confocal microscopy. Of note, in cultured organoids, the apical side faces the interior (lumen) of the sphere, while the basal surface is towards the exterior (supporting matrix). ZO-1 was located at the apical boundary of intestinal epithelial cells under normal glucose conditions and pre-treatment with HA35 did not alter this arrangement (**Fig. 2A**). However, high glucose conditions disrupted the normal localization of ZO-1, and pre-treatment with HA35 prevented this loss (**Fig. 2A**). This ZO-1 staining, and expression pattern was also observed in monolayers (**Supplemental Fig. 2**, ZO-1 shown in grayscale). Occludin staining was observed lining the outer boundary of individual epithelial cells under normal glucose conditions both in the absence and presence of HA35 pre-treatment (**Fig. 2B**). Under high glucose conditions, larger cells with decreased occludin staining between cell boundaries were observed (**Fig. 2B**, inset), and pre-treatment with HA35 prevented this change (**Fig. 2B**). Like ZO-1, claudin-1 staining was localized at the apical surface of the cells in organoids grown in normal glucose with or without HA35 (**Fig. 2C**). We also observed that the apical organization of claudin-1 was disturbed under high glucose conditions but pre-treatment with HA35 was not protective (**Fig. 2C**). Together, imaging studies show that in addition to preventing protein loss, pre-treatment with HA35 specifically maintains the spatial distribution of both ZO-1 and occludin under high glucose conditions.

To address the question of whether the effect on junction protein disruption was specific to glucose or alternatively a function of the higher osmolarity of the media leading to barrier

impairment, we compared cultured organoids treated with 25 mM mannose to those treated with 25 mM glucose following pre-treatment without or with HA35. No changes in the spatial distribution of ZO-1 were observed in organoids treated with mannose indicating that barrier impairment under high glucose conditions is not simply a result of osmotic stress but is a specific response (**Supplemental Fig. 3A**).

We have previously shown in detail that HA35 has specific effects on intestinal cells not shared with larger molecular weight HA species [23, 26, 27]. To confirm that the barrier protective effects observed in these studies are also specific to low molecular weight HA, organoids were pre-treated with 2000 kDa molecular weight HA (HA2000) and challenged with normal and high glucose medium. HA2000 pre-treatment was not protective in maintaining ZO-1 expression at the epithelial barrier surface under hyperglycemic stress (**Supplemental Fig. 3B**) suggesting specificity of HA size, consistent with data from prior *in vitro* and *in vivo* models [26, 27].

HA35 protects functional barrier integrity under hyperglycemic stress

To determine whether hyperglycemic stress also alters functional barrier permeability in intestinal organoid cultures, and whether HA35 protects from any disruption, additional assays to measure the tightness of the barrier interface were performed. Two widely acceptable *in vitro* systems were utilized for this assessment including Fluorescein isothiocyanate (FITC)-dextran permeability measurements and measurement of transepithelial electrical resistance (TEER). Note, intestinal organoids were flipped inside out with the apical surface facing outward using a protocol published by Co et al [35] for these studies. Flipped organoids were pre-treated without or with HA35 (24 hours) followed by addition of normal or high glucose medium. FITC-dextran (40 kDa) was added to the organoids 48 hours after high glucose treatment. Organoids were imaged using a confocal microscope one hour after FITC-dextran addition to determine the exclusion of the probe. Qualitative results showed that while low amounts of 40 kDa FITC-dextran penetrated the organoids grown in 5 mM glucose as well as in organoids pre-treated with HA35 under normal glucose conditions (**Fig. 3A**), these organoids mostly had dark centers when visualized in the Alexa 488 (green) immunofluorescence channel. Increased FITC-dextran penetration was observed in organoids treated with high glucose, i.e. organoid centers were fluorescent green indicative of impaired barrier or increased FITC transit in this treatment group (**Fig. 3A**, black arrows). Pre-treatment with HA35 decreased FITC-dextran transit under high glucose conditions. The number of organoids with dark centers in each treatment group was counted. Results showed that hyperglycemic stress alters the barrier permeability (**Fig. 3B**). While pre-treatment with HA35

under high glucose conditions did not completely normalize the barrier permeability, HA35 improved the barrier in comparison to organoids treated with high glucose alone (**Fig. 3B**).

We performed an additional assay, trans-epithelial electrical resistance (TEER) measurement, to assess the barrier permeability in the intestinal epithelium in the four treatment groups. Intestinal epithelial monolayers were grown from organoids on transwell inserts in normal glucose media. Monolayers were treated without or with HA35 and subsequently exposed to normal or high glucose in a similar fashion to the three-dimensional intestinal organoids (**Fig. 1A**). TEER was measured every 24 hours during the treatment regimen. Baseline TEER measurements were made on day 0, before the addition of HA35. TEER values measured on subsequent days were normalized to values of individual wells measured at the start of the experiment (day 0). Control (normal glucose) monolayers maintained their TEER values closer to baseline reading on day 3 at 88.9% compared to high glucose treatment (**Fig. 3C**). Monolayers treated with high glucose steadily declined in TEER reading over the baseline set at 100% with final reading of 69.3% on day 3 indicating that hyperglycemic stress increases barrier leakiness (**Fig. 3C**). Monolayers pre-treated with HA35, both normal and high glucose treated, steadily increased in TEER values indicative of a tighter barrier interface (**Fig. 3C**). Taken together, this data shows that HA35 not only maintains the spatial distribution of key tight junction proteins under high glucose conditions, but also prevents functional impairment of intestinal permeability under hyperglycemic stress.

HA receptor, layilin, is involved in the HA35 mediated maintenance of barrier integrity under hyperglycemic stress

Intestinal epithelial cells express several receptors required for HA signaling that play a critical role in barrier defense mechanisms. To determine which receptors are involved in preventing the loss of barrier proteins under high glucose conditions in the presence of HA35, we grew organoids from mice that were deficient in known receptors required for HA signaling, including layilin, toll-like receptor 2 (TLR2), TLR4, and CD44. We performed immunofluorescence staining and quantified protein expression of ZO-1 as an initial screen to identify the key receptors. Results showed high glucose reduced ZO-1 protein expression but HA35 pre-treatment did not prevent loss of ZO-1 in organoids grown from layilin knockout (LAYN-/-) mice (**Fig. 4A**). Confocal imaging results also showed reduced expression of ZO-1 protein under hyperglycemic stress with or without HA35 treatment in LAYN-/- organoids (**Fig. 4C**). In all other genotypes (TLR4-/-, TLR-/-, CD44-/-), we observed visually that high glucose reduced apical staining of ZO-1 with visible patterns of disruption (**Supplemental Fig. 4A**). While it appeared that HA35 pre-treatment

preserved the expression of ZO-1 in these genotypes under high glucose conditions (confocal images), data obtained from western blot analysis did not show any changes across the four treatment groups (**Supplemental Fig. 4A, B**). Because results obtained from spatial distribution and quantification of ZO-1 protein expression were inconclusive in TLR4-/-, TLR2-/- and CD44-/- mice, we focused on layilin as an important receptor involved in barrier protective effects of HA35. Next, protein expression of occludin was quantified in LAYN-/- organoids and no differences were observed across the four treatment groups (**Fig. 4B**). While qualitatively assessing the spatial distribution of occludin in LAYN-/- organoids, we observed that large proliferative cells, similar to those seen in high glucose wild-type organoids, were present in normal glucose controls treated with or without HA35 (**Fig. 4D**, white arrows). In these areas, the expression of occludin was low compared to cells that were a normal size. However, it appeared that in high glucose conditions, LAYN-/- organoids had an increased disruption of ZO-1 staining (**Fig. 4D**). Several areas of disruption in occludin staining were also identified in organoids pre-treated with HA35 followed by high glucose exposure (**Fig. 4D**). Interestingly, the areas with reduced ZO-1 staining also corresponded with diffuse E-cadherin staining, which was most prominent in the high glucose group (**Fig. 4D**, bottom panel). Based on the screen of various receptors, it appeared that layilin plays a prominent role in the barrier protective effect of HA35 under hyperglycemic stress.

HA35 regulates cell death and survival under high glucose stress

To help determine the underlying molecular mechanisms involved in the protective effect of HA35 under high glucose conditions, we utilized an untargeted proteomics approach. Proteomics data was utilized to perform pathway analysis to identify top pathways upregulated in the experimental treatment groups. Comparison of organoids pre-treated with HA35 in high glucose conditions with organoids grown in high glucose alone showed cell death and survival, cellular development and cell growth and proliferation as top three pathways upregulated with HA35 pre-treatment under high glucose stress ($p<0.05$) (**Fig. 5A**). Next, we analyzed all the top up- and downregulated proteins quantified using untargeted proteomics analysis ($p<0.05$). Proteins that were highly up- or downregulated (100-fold or higher) under high glucose stress in comparison to normal glucose controls included Xaf1, Polr1f, Slc44a4, and Usp12 (**Fig. 5B**). Of these four candidate proteins, Xaf1, a key player in cellular apoptosis, was down-regulated over 400-fold under high glucose conditions compared to normal glucose treatment controls at 48 hours post-treatment (**Fig. 5B**). Xaf1 is a proapoptotic tumor suppressor that binds to and counteracts the effect of proteins that are members of inhibitor of apoptosis (IAP) protein family, thereby restoring normal apoptotic cell death mechanisms [36]. Since cell death and survival was a top pathway regulated by HA35 pre-

treatment under high glucose conditions, we focused on understanding the regulation of Xaf1 by HA35. To confirm whether changes in Xaf1 protein occurred early in the treatment timeline, we performed immunoblotting analysis. A time course protein immunoblot experiment was set up to analyze cell lysates at 30 minutes, 1 hour, 2 hours and 4 hours post-treatment (**Fig. 5C**). Pre-treatment with HA35 followed by addition of high glucose increased cellular Xaf1 protein compared to untreated controls (30 minutes) as well as cells treated with HA35 alone (30 minutes and 2 hours) (**Fig. 5D**). Additionally, the increase in cellular Xaf1 protein was dependent on layilin since Xaf1 protein was downregulated in LAYN-/- organoids pre-treated with HA35 (1, 2, and 4 hours) under high glucose stress compared WT controls (**Fig. 5E**). These results show that under high glucose conditions, HA35 pretreatment upregulates the expression of Xaf1, which is dependent on the presence of the HA receptor layilin. These observations led us to evaluate whether apoptotic mechanisms were impaired under hyperglycemic stress and to test whether HA35 pre-treatment alters this cellular process.

HA35 counteracts the effect of hyperglycemic stress on apoptotic cell death

To determine the impact of high glucose stress and HA35 on cell death and survival mechanisms, we assessed proteins involved in apoptotic cell death mechanisms. Proteomics analysis and western blotting did not show any changes in the proteins tested, including caspases involved in apoptosis across the four treatment groups (**Supplemental Fig. 5A, B**). This may be artifact of sample preparation, since apoptotic cells typically accumulate in the lumen of the organoid towards the center, and sample preparation for protein analysis utilized specialized buffers to remove dead cells. Therefore, to better visualize the number of dead cells that express cleaved caspase 3, a marker of programmed apoptotic cell death, we performed whole mount organoid immunofluorescence staining followed by confocal microscopy. Staurosporine was used as a positive control (**Supplemental Fig. 5C**). We observed that under normal glucose conditions, dead cells stained with cleaved caspase 3 accumulate in the luminal space of the organoids, and pre-treatment with HA35 does not alter this staining pattern (**Fig. 6A**). However, under high glucose conditions, qualitatively the number of cells stained with cleaved caspase 3 is much lower compared to normal glucose. (**Fig. 6A**). In organoids pre-treated with HA35 followed by high glucose, we observed more apoptotic cells in the lumen compared to high glucose treatment alone (**Fig. 6A**). Flow cytometric analysis of organoid derived cells was performed to quantify ones undergoing apoptosis demonstrated that addition of high glucose reduced the numbers of apoptotic cells and pre-treatment with HA35 maintained these numbers at near baseline compared to the control groups (**Fig. 6B**). We also assessed proliferation by performing

immunofluorescence staining and flow cytometry analysis. Visually, we observed that the numbers of Ki67 (marker for proliferation) positive cells were higher in organoids treated with high glucose compared to control groups (**Supplemental Fig. 6A**). Pre-treatment with HA35 decreased the number of Ki67 positive cells under high glucose conditions as observed by confocal imaging (**Supplemental Fig. 6A**). Flow cytometry analysis mirrored the results from confocal imaging. High glucose treatment increased proliferation (% Ki67 positive cells) compared to both normal glucose groups (**Supplemental Fig. 6B, C**). Pre-treatment with HA35 dampened the proliferation driven by hyperglycemic conditions but not to the total numbers measured in control normal glucose groups without or with HA35. (**Supplemental Fig. 6B**).

These observations begged the question of whether absence of the layilin receptor altered apoptosis in organoids grown from LAYN-/- mice. To this end, we performed immunofluorescence imaging as well as flow cytometry to qualitatively and quantitively evaluate cleaved caspase 3 in LAYN-/- organoids. Results showed that cleaved caspase 3 expressing cells were decreased in both high glucose groups (with and without HA35) compared to 5 mM controls as seen in representative confocal images (**Fig. 6C**). Flow cytometry analysis showed that high glucose decreased the percentage of apoptotic cells in comparison to control and pre-treatment with HA35 was unable to restore apoptosis to baseline control (**Fig. 6D**). These results demonstrate that normal apoptotic cell death as well as proliferation is altered in intestinal epithelial cells under hyperglycemic stress. Taken together, these results demonstrate that pre-treatment with HA35 under high glucose stress not only increases the levels of the pro-apoptotic tumor suppressor, Xaf1, but also maintains a balance of essential cellular processes (apoptosis, proliferation) in epithelial cells. Functional changes in these cellular processes have been previously linked to barrier protein degradation or loss in inflammatory bowel disease [37], and colon cancer [38, 39]. HA35 pre-treatment normalizes high glucose induced apoptotic changes, and as noted, layilin seems to be a central player in the barrier protective effects of HA35.

HA35 maintains spatial distribution of F-actin and focal adhesion kinase (FAK) via layilin under high glucose conditions

Layilin, a C-type lectin domain-containing membrane glycoprotein, is thought to bridge the interactions between ECM components, such as HA, and the cellular cytoskeleton (such as F-actin) via the layilin-talin-integrin-FAK axis [40-43]. Recent studies have shown that FAK plays a key role in maintenance of the intestinal epithelial barrier [44]. Based on our observation that layilin is key to maintenance of the barrier under high glucose stress in the HA35 pre-treated organoids, we quantified key proteins in the layilin-talin-integrin-FAK pathway utilizing untargeted

proteomics (**Supplemental Table 1**). We did not observe any changes in the total expression of proteins including Ptk2 (focal adhesion kinase 1), talins 1 and 2, paxillin, Actb (actin, cytoplasmic 1), and several integrins at the 48-hour time point post-high glucose treatment. Next, we assessed the spatial organization of F-actin (phalloidin) and total FAK at an earlier time point (24 hours) post-high glucose treatment in organoids derived from wild-type as well as LAYN-/- mice. F-actin (phalloidin staining) was mainly located at the apical surface of the intestinal epithelial cells and co-localized with ZO-1 expression in organoids grown in normal glucose conditions (± HA35 pre-treatment) (**Fig. 7A**). FAK expression was localized to apical, basolateral, as well as inter-epithelial cell boundaries in normal glucose controls (± HA35 pre-treatment) (**Fig. 7A, 7B**: FAK inset). Similar localization of FAK has been observed previously in Caco2 monolayers [44]. Addition of high glucose (25 mM) disrupted the spatial distribution as well as expression of ZO-1, F-actin, and FAK (**Fig. 7A, 7B**: FAK inset). Pre-treatment of wild-type organoids with HA35 for 24 hours prior to high glucose addition maintained the spatial organization of ZO-1, F-actin, and FAK suggesting that this specific downstream mechanism might be key to maintaining the epithelial barrier (**Fig. 7A, 7B**: FAK inset).

Next, we examined whether the HA receptor, layilin, was critical in maintaining the spatial distribution of F-actin and FAK in LAYN-/- intestinal organoids. Spatial organization of ZO-1, F-actin, and FAK, similar to that observed in wild-type organoids, was preserved in LAYN-/- organoids under normal glucose conditions with and without HA35 pre-treatment (**Fig. 8A, B**: FAK inset). However, HA35 pre-treatment did not rescue this effect under high glucose stress (**Fig. 8A, B**: FAK inset). This suggests that layilin is critical to activate signaling mechanisms downstream of HA-layilin interactions in the maintenance of epithelial barrier including FAK as well as F-actin organization in intestinal epithelial cells.

Discussion

Our study shows that increased glucose concentration, even in acute exposure, can induce barrier damage and alter normal cellular apoptotic mechanisms in the intestinal epithelium. In this study we demonstrate that organoid tight junction protein ZO-1 arrangement, and function are altered under high glucose stress. Additionally, our current data using HA35 expands on our previous reports [26, 27, 32, 45] by suggesting that HA35 exerts a protective role in the intestine by regulating barrier function under high glucose stress. More importantly, using mechanistic tools such as proteomics analysis, we show that while high glucose alone alters cellular apoptosis by decreasing Xaf1 protein concentration, HA35 treatment of intestinal organoids increases Xaf1 protein expression to restore apoptosis to near baseline (control) numbers. In addition, we

demonstrate that HA35 likely acts through its receptor, layilin, to activate the layilin-integrin-FAK axis since we observe altered spatial distribution and expression of FAK and F-actin in organoids pre-treated with HA35 in comparison to high glucose treatment. These observations correlate with prior findings that show altered cellular processes including cellular metabolism, apoptosis, proliferation impact barrier integrity in intestinal disease, specifically colon cancer [45-50]. Our study also demonstrates the importance of maintaining balance between proliferation vs. apoptotic cell death, and how changes in these processes under high glucose stress alters barrier permeability. Given the increased incidence of IBD and colorectal cancer in patients with hyperglycemia, our results highlight the importance of a high sugar diet as well as metabolic syndrome on intestinal barrier dysfunction.

The impact of hyperglycemic stress has been investigated by other groups utilizing various *in vitro* as well as *in vivo* model systems. In a recent study by Dubois et al., monolayers grown from Caco2 and HT29-HTX (both human colon cancer cell lines with epithelial morphology) cells were treated in high glucose (25 mM) conditions for 21 days [22]. During this treatment period, several transcriptional, protein content, and spatial changes in junctional proteins (ZO-1, occludin, E-cadherin) were measured, which corresponded with decreased TEER measurements in both cell lines under high glucose conditions [22]. However, the exact mechanism by which high glucose altered junctional complexes in these cell lines was unclear. Animal models have been widely used to understand mechanisms of either diet-induced or obesity-induced disruption of homeostatic mechanisms in the gut with a focus on barrier integrity [21, 45, 51]. Wild-type (C57BL/6) mice fed 15% glucose (in water) were shown develop a greater increase in paracellular permeability in the upper intestinal tract (jejunum and cecum) in comparison to mice provided 15% fructose (in water) regimen [51]. The loss of barrier function was attributed to changes in gut microbial diversity, specifically enrichment of *Lachnospiracae* and *Desulfovibrionaceae* species [51]. In a study performed using animal models of obesity, db/db mice and high-fat diet feeding regimen, Thaiss et al., reported an increase in enteric infection due to changes in intestinal barrier permeability as measured by decreased ZO-1 expression in mouse colons [21]. They also demonstrated that barrier dysfunction was a result of hyperglycemic stress in mice, and that glucose transporter 2 (GLUT2) was involved in epithelial reprogramming under high glucose conditions [21]. In mice where GLUT2 was deleted specifically in epithelial cells, decreased Citrobacter rodentium infection as well as improved barrier function was observed [21]. While the above *in vivo* animal studies highlight the impact on metabolic stress on barrier function, multiple confounding factors in addition to high glucose such as the microbiome composition, immune cells, cytokine/chemokines, and adipokines might be at play as well.

Our study found that HA35 treatment restored cellular death and survival mechanisms under high glucose stress. Specifically, we found that HA35 treatment increased protein expression of Xaf1 under high glucose conditions, a protein that has been shown to regulate cellular apoptosis. Xaf1 has been studied as a pro-apoptotic tumor suppressor that neutralizes the anti-caspase activity of XIAP to normalize cellular apoptotic functions [52]. Members of the IAP protein family, such as XIAP, bind to and inhibit caspases that are activated during apoptosis, thereby impairing normal apoptotic cell death [53]. In pathological conditions, such as prostate cancer, it was found that Xaf1 expression was downregulated, thereby accelerating tumorigenesis [54]. Cell junctional proteins, such as ZO-1 and occludin, have been traditionally studied for their important role in barrier maintenance in the intestine. However, recent studies have highlighted the noncanonical function of these proteins in epithelial cell proliferation and apoptosis [37, 55-57]. Specifically, both ZO-1 and occludin have been shown to regulate mucosal repair mechanisms in IBD by modulating mechanisms of epithelial cell survival. Interestingly, in patients with Crohn's disease, the degree of caspase 3 downregulation directly correlated with that of occludin protein expression highlighting the clinical relevance of a key barrier protein in apoptotic cell death [58]. In our study, it seems likely that high glucose conditions impact both canonical as well as noncanonical functions of these barrier proteins, processes that HA35 pretreatment can largely mitigate.

The protective effect of HA35 in the organoid model appears to be mediated, at least in part, by the receptor layilin on epithelial cells. Layilin is a C-type lectin receptor that recognizes low molecular weight HA, including HA35 [27, 31]. Prior studies in animal models of intestinal injury have shown that layilin is critical for the barrier protective effects of HA35 [27, 31]. Layilin signaling has been studied in the context of barrier function. Layilin also participates in intracellular interactions with cytoskeletal proteins such as talin, vinculin, actin, and focal adhesion kinase (FAK) that are involved in cytoskeletal activation [59]. Among these cytoskeletal proteins, FAK was identified to be a key component of the ZO-1/occludin complex that regulates the intestinal barrier [44]. We speculate that HA35 regulates cytoskeletal protein signaling via layilin, thereby leading to altered barrier function as well as spatial rearrangement of barrier proteins, ZO-1 and occludin. In addition to barrier function, cytoskeletal proteins such as FAK that are regulated by layilin signaling also play a role in epithelial cell survival, proliferation, and migration [60]. In this study we showed that in the absence of layilin, HA35 mediated effects on normalizing apoptosis responses under hyperglycemic stress were much reduced compared with wild-type organoids. We observed that effects of HA35 on upregulation of Xaf1 protein expression were also absent in layilin knockout organoids. Finally, we showed that spatial organization of both FAK as well as F-

actin is mediated by HA35 via layilin. This suggests a link between regulation of epithelial cell maintenance of barrier and cellular apoptosis modulated via layilin-integrin-FAK axis in the presence of HA35 (**Fig. 9**).

Despite the intriguing glucose stress mediated epithelial cell changes uncovered, and their mitigation by HA35, there are always limitations to extrapolating from *in vitro* to organismal functioning. Undoubtedly *in vivo*, the complexity of the biological milieu (microbiome, immune cells, hormones, cytokines/chemokines, adipokines, lipids), cellular crosstalk, and other components of the matrix (fibronectin, proteoglycans etc.) play a vital role in intestinal barrier function during metabolic inflammation. Also, while proteomics-based analysis allowed us to identify at least one protein that is involved in modulating apoptosis in intestinal organoids in the presence of HA35, there are other pieces to this puzzle that are yet unexplored. For example, still unknown is whether cytoskeletal proteins, in addition to actin, that form complexes with barrier proteins such as ZO-1 and occludin undergo changes in the high glucose environment or in the presence of HA35. In addition, we have not fully explored the noncanonical functions of barrier proteins and their mechanistic role in cellular processes such as apoptosis under high glucose stress.

As a final technical caution, in identifying the compromising effect of glucose on epithelial junctions, we realized that many cell culture systems typically use growth medium that is in the high glucose range. For example, as reported in manufacturer product information, DMEM (Hi), GMEM and IMDM all contain 25 mM concentration of D-glucose. H-Y Medium (Hybri-Max®) and Serum-Free/Protein Free Hybridoma Medium contain 22.6, and 28.9 mM D-glucose, respectively. Our group's original paper showing ZO-1 in organoids used a DMEM (Hi) medium formulation for growth and control conditions, as recommended in the literature. The ZO-1 expression we reported previously [27] was blunted compared with normal glucose treatments in this study. Quite likely, many other investigators are conducting experiments with cells that are already glucose-stressed and may be getting quantitatively altered cell responses.

Our *in vitro* studies permitted the examination of intestinal epithelial cellular and molecular mechanisms in genetically matched murine cells. The presented data highlights, for the first time, a direct role of hyperglycemic stress on normal, primary epithelial cell barrier integrity and function via modulation of a key protein that participates in apoptotic cell death. We also demonstrate the barrier protective effect of HA35 involves regulating apoptosis as well as proliferation in intestinal organoids occurs in conjunction with upregulation of the protein, Xaf1, and via modulation of the layilin-integrin-FAK axis. Results from this study emphasize that diet modifications, specifically

long-term high sugar diet consumption, to lead the development of intestinal diseases through impairment of barrier function. Since dietary HA35 is clinically tolerable, there is potential for translation from these preclinical findings to application in patients with metabolic syndrome.

Materials and Methods

Animals

All animal procedures were reviewed and approved prior to initiation by the Cleveland Clinic Institutional Animal Care and Use Committee. All animals utilized in the study were on a C57BL/6J background. Wild-type C57BL/6J (Stock No: 000664), 8–12-week-old animals were purchased from Jackson Laboratories. TLR2-/- (Stock no: 004650), TLR4-/- (Stock No: 029015), and CD44-/- (Stock No: 005085) deficient mice were also purchased from Jackson Laboratories. Transgenic layilin knockout (LAYN-/-) previously on C57BL/6N background mice were crossed onto a C57BL/6J background in house. Based on the single nucleotide polymorphism (SNP) analysis used by Jackson laboratories to characterize sub-strain background, we were able to achieve 100% C57BL/6J background in LAYN-/- animals. Both male and female mice were equally distributed in the various treatment groups in this study. Mice were fed standard rodent chow and co-housed (4 animals/cage) in a micro-isolator cage prior to experimental use.

Intestinal crypt isolation and organoid culture

Specific recipes for organoid wash buffer, organoid growth media, differentiation media, and monolayer growth media have been detailed in **Supplemental Table 2**. Intestinal crypts were isolated from distal colons and cultured according to previously published protocols by Miyoshi and Stappenbeck [34]. Briefly, colonic tissue was harvested from mice and cut into small pieces (0.5 cm x 1.0 cm). Tissue pieces were minced and digested in 1.8 ml of collagenase I solution (2 mg/ml, Gibco, 17100-017) containing 50 U/mL gentamicin (Gibco, 15750-060) prepared in organoid wash buffer for 10 minutes at 37℃. Tissue was re-suspended vigorously in the collagenase solution using a P1000 pipette to break the crypts away from the colon tissue. The incubation and re-suspension steps were repeated until 70-80% of the crypts were released from the tissue. Tissue digest was filtered (100 µm pore filter, Falcon cell strainer, 352360), centrifuged (50-80 g for 5 minutes), and clumps of cells (clumps with 3 or more cells) were counted before organoid plating. Approximately 5000 crypt units were resuspended in 15 µl of Matrigel (Corning, 356231). Matrigel domes (3-6 domes/well) were plated in 12-well Corning tissue culture plates (Corning, 3512). Tissue culture plates were placed in the incubator (37℃, 5% CO_2) for 15-30 minutes to allow the Matrigel to solidify. L-WRN conditioned media [61] (50%, 1 mL/well) containing 100 µM Rho/ROCK inhibitor Y-27632 (Tocris, 1254) as well as 500 nM ALK inhibitor A-83-01 (Tocris, 2939) was added to each well. Media concentration was maintained at 5 mM during organoid expansion. Glucose concentration was adjusted using a Germaine glucometer (AimStrip Plus blood glucose meter, 37321). Organoid maintenance protocol was adapted from Sato et al

[62]. Half the media was replaced every two days allowing the organoids to grow until they were ready to be split for experimental set up. Media concentration was maintained at 5 mM glucose during the growth and expansion phase of the organoids.

In Vitro Experimental set up for downstream assays

Highly purified, certified endotoxin free sodium hyaluronate or hyaluronic acid (HA35 and HA2000) was purchased from Lifecore Biomedical LLC. For *in vitro* experiments, HA was dissolved by shaking at 4℃ overnight in distilled (sterile) water at 2 mg/mL concentration. The experimental set-up for various downstream assays has been shown in **Fig. 1A**. Briefly, organoids were trypsinized and re-suspended in Matrigel (5000 crypt units in 15 µl Matrigel). Organoid domes were plated on day 0 at 3 domes/well of a 12-well plate. After Matrigel solidification, 1 ml of 50% L-WRN (without Y-27632 and A83-01) at 5 mM glucose concentration was added to each well. Every other day media was replaced with half the volume (0.5 ml) of fresh 50% L-WRN (without Y-27632 and A83-01) and concentration was maintained at 5 mM glucose. On day 6, HA pre-treated wells received 350 µg/ml of HA35 in addition to media refreshment. After a 24-hour period, all wells received a complete media change on day 7 and a fresh dose of HA35 in the appropriate wells. Organoid wells were split up into four distinct treatment groups: 1) 5 mM glucose media, 2) 5 mM glucose media and HA35 pre-treatment, 3) 25 mM high glucose media, and 4) 25 mM high glucose media and HA35 pre-treatment. For most experiments, except time courses, cells were harvested at 24 hours or 48 hours post-treatment on day 9. For time course experiments, cells were harvested at 30 minutes, 1 hour, 2 hours, and 4 hours after treatment.

Western blot

Organoids were harvested in cell recovery solution (Corning, 354253) on ice and P1000 pipette was used to break the organoids from Matrigel followed by centrifugation (500xg, 5 minutes). Cell pellets were washed twice in ice cold 1X phosphate buffered saline (PBS) followed by centrifugation (500xg, 5 minutes). For western blot experiments, cell pellets were re-suspended in 250 µl RIPA lysis and extraction buffer (ThermoFisher Scientific, 89900) containing protease and phosphatase inhibitors (ThermoFisher Scientific, 1861281). Samples in RIPA buffer were incubated on ice for 20 minutes with vigorous vortexing every 5 minutes. A final centrifugation was performed (10000 rpm, 10 minutes) and supernatant was transferred for storage at -80℃ until further use. Protein concentrations were measured using Pierce BCA Protein assay (ThermoFisher Scientific, 23225). Protein samples were mixed with lithium dodecyl sulfate (LDS, Invitrogen, NP0007) and sample reducing agent (Invitrogen, NP0009). After boiling at 100℃,

proteins were separated using SDS-PAGE with 4-12% NuPAGE Bis-Tris protein gels (Invitrogen, NP0323BOX) at 200V for 60-90 minutes. Depending on the protein size, 1X MOPs (Invitrogen, NP0001) or 1X MES buffer (Invitrogen, NP0002) was used for protein separation. Separated proteins were transferred at 4℃ to 0.45 µm PVDF membrane (Millipore, 1PVH00010) in a solution of 1X Tris Glycine buffer (ThermoFisher Scientific, 28362) containing 20% methanol at 30V overnight. PVDF membranes were blocked in PBST (PBS with 0.1% Tween 20) containing 5% milk for 1 hour. Membranes were probed with antibodies using manufacturer's protocol. The following antibodies were used for experiments: ZO-1 (ThermoFisher Scientific, 61-7300), claudin-1 (ThermoFisher Scientific, 71-7800, occludin (ThermoFisher Scientific, 40-4700), XAF1 (Abcam, ab17204), caspase 3 (Cell Signaling, 9662S), and GAPDH (Cell Signaling, 2118S). Densitometry and quantification of protein expression was performed using Image J software (Version 1.54i). Individual protein expression was normalized to loading controls (GAPDH).

Quantitative real time PCR analysis

For qRT-PCR experiments, cell pellets were collected in Corning cell recovery solution as described above. Cell pellets were resuspended in RLT buffer (350 µl) containing beta mercaptoethanol (Gibco, 21985-023) and RNA extraction was performed according to manufacturer's instructions using Qiagen RNeasy Mini Kit (Qiagen, 74004). RNA was converted to cDNA using the Bio-Rad iScript cDNA synthesis kit (Bio-Rad, 1708891). qRT-PCR was performed in triplicate using iQ SYBR Green supermix (Bio-Rad, 170-8882) and quantified using the $2^{-\Delta\Delta CT}$ method.

Whole mount immunofluorescence staining and confocal imaging

To harvest organoids for whole mount staining, 15 mL conical tubes were coated with anti-adherence buffer (1% bovine serum albumin-BSA in 1X PBS) to prevent clumping. Wide pore P1000 pipette tips coated with anti-adherence buffer were used to gently scrape Matrigel domes containing organoids from culture plates in Corning cell recovery solution (ice-cold). During harvest, domes were broken up by gentle pipetting to release organoids from Matrigel. 15 mL conical tubes containing organoids in cell recovery solution were placed on a rocker (horizontal configuration) on ice at 4℃ for 1 hour to remove Matrigel. Organoids were allowed to settle by gravity at room temperature and supernatant was removed gently without disturbing the pellet. Next, 2 mL 4% paraformaldehyde (PFA, Alfa Aesar, J61899.AP)) was added to each tube to fix the organoids. Tubes were incubated on ice for 1 hour at 4℃ on a rocker (horizontal configuration). After 1 hour fixation, organoids were allowed to settle by gravity, supernatant was

removed and 2X washes were performed using 10 mL 1X PBST (0.1% Tween 20 in 1X PBS). Supernatant was removed and 2 mL blocking/permeabilization buffer (1X PBS, 0.2% Triton-X100, 2% BSA, 5% FBS) was added to each tube. Samples were transferred to a 24-well anti-adherence culture plate (Corning, 3473) for the subsequent steps using a wide bore pipette tip. Culture plate containing organoids was blocked for 1 hour at room temperature on a rocker followed by gravitational settling of organoids by tilting the plate at a 45˚ angle on a stand. Excess blocking buffer was removed gently. Primary antibodies were added at 1:400 concentration (200 µl/well) in blocking buffer. The following primary antibodies were used for staining: ZO-1 (ThermoFisher Scientific, 61-7300), claudin-1 (ThermoFisher Scientific, 71-7800, occludin (ThermoFisher Scientific, 40-4700), E-cadherin (ECM Biosciences, CM1681), Ki67 (Abcam, ab15580), cleaved caspase-3 (Cell Signaling, 9661S), and focal adhesion kinase (FAK) (Proteintech, 66258-1-Ig). Appropriate IgG controls were used to optimize staining (**Supplemental Fig. 8**). Cells treated with Staurosporine (Tocris, 1285) was used as a positive control for cleaved caspase-3 staining. Overnight incubation in primary antibody was performed on a rocker at 4℃. Next day, gravitational settling was performed as described above (45˚tilt angle) and excess supernatant was removed. Washes in blocking buffer (1 mL/well) were performed 3 times for a duration of 2 hours/each wash (24-well plate placed on rocker for the 2-hour duration). Secondary antibodies (1:1000 dilution, anti-rabbit Alexa 568 and anti-mouse Alexa 633) were added in blocking buffer and incubation was performed overnight at 4℃. Alexa Fluor 488 Phalloidin (ThermoFisher, A12379) was added with secondary antibodies to stain for F-actin. Next day, a quick wash step was performed in 1X PBS followed by DAPI staining for 30 minutes. Two-hour long washes (3X) were performed in 1X PBS. After the last wash, organoids were mounted on slides using clearing solution (2.5 M fructose in 60% glycerol). Images were obtained using an inverted Leica SP8 confocal microscope using 40X oil objective lens at 1X zoom factor, unless otherwise specified (for insets). Images acquired in Alexa 633 channel were pseudo-colored green after acquisition.

Reversing polarity in organoids for FITC-dextran flux assay

Apical-out organoid cultures were used to measure FITC-dextran flux. The protocol for polarity reversal of organoids was adapted from Co et al [35]. Briefly, on day 0, five densely populated Matrigel domes containing organoids were collected for each experimental well containing flipped organoids. For example, for a total of 4 treatment groups per mouse, 20 domes were collected. Spheroid domes were scraped and suspended in ice cold 1X PBS containing 5 mM EDTA (Invitrogen, 15575-038). The solution containing organoid domes was rocked in a cold room at 4℃ for 1 hour. Cells were collected by centrifugation (300xg, 3 minutes). The pellet was

resuspended in organoid wash buffer and centrifuged to collect cells (300xg, 3 minutes). Cells were plated for experimental use in differentiation media in Corning Ultra-low attachment plates (Corning, 3473). Similar treatment groups (4 groups) as described above were utilized in this assay. HA35 (350 µg/ml) pre-treatment was added to the appropriate wells on day 2 after media change. High glucose (25 mM) was added to designated wells on day 3. Flipped organoids were collected 48 hours post-high glucose treatment in gentle cell dissociation buffer (Gibco, 13151-014) and incubated for 10 minutes (room temperature). After centrifugation (200xg, 5 minutes), organoid pellets were re-suspended in 40 kDa FITC-dextran (200 µl, concentration 1 mg/ml, Invitrogen, D1845) for 5 minutes. Organoids were allowed to settle by gravity followed by removal of supernatant. Organoids were transferred to a slide for confocal imaging. Images were obtained using an inverted Leica SP8 confocal microscope using 40X oil objective lens at 1X zoom factor.

Transepithelial electrical resistance (TEER) measurement

Organoids were grown for two passages in monolayer growth media prior to seeding the transwells. To seed monolayers, transwells (6.5 mm, 0.4 µm pore, clear polyester) were pre-coated with 10% Matrigel. Approximately 15 Matrigel domes containing organoids were harvested in dissociation buffer. Dissociation buffer contained 0.5 mM EDTA (Invitrogen, 15575-038) and 1 µM DTT (Sigma Aldrich, D0632) in 1X PBS. After centrifugation (335xg, 5 minutes), organoids were resuspended in 1.0 ml of TrpLE Express (Gibco, 12604-021) and incubated for 5 minutes at 37℃. After incubation, 1 mL wash buffer was added and clumps of cells were counted (2-4 cells/clump, not including single cells) using trypan blue exclusion. Approximately 15,000-35,000 clumps/insert were plated in the top chamber of the transwell (Corning, 3470) in 150 µl of monolayer growth media. After the monolayers were confluent (2-3 days), media was switched differentiation media and HA35 (350 µg/ml) pre-treatment was added. High glucose treatment (25 mM) was added 24 hours later to the appropriate wells. TEER was measured for individual treatment groups every 24 hours throughout the duration of the assay.

Untargeted proteomics analysis

To lyse the cells, 150 µl 8M urea 0.1M Tris-HCl pH 8.0 with protease inhibitor cocktail was added to each sample. The samples were homogenized on a sonicator at 40% amplitude using 3x 10s pulses with 10s between pulses. Homogenized samples were centrifuged 21kg for 20 mins at room temperature and a small aliquot from each supernatant were diluted 5x with water and used for a BCA protein assay. Forty µg of protein from each of the samples were taken based on BCA results. The samples were reduced by dithiothreitol, alkylated by iodoacetamide and precipitated

by cold acetone (-20°C) overnight. Samples were centrifuged at 12000 g for 8 minutes at 0 °C, and the supernatants were removed. Protein pellets were air dried for 30 minutes and dissolved in 40 µL 100 mM tri-ethyl ammonium bicarbonate (TEAB) with 0.5 µg trypsin per sample. After overnight incubation, digested samples were centrifuged at 21 kg for 15 minutes, and 5 µg of the digest from each sample was transferred to a new tube and dried down in a SpeedVac and reconstituted in 25 µl 0.1% formic acid. Ten µl sample was mixed with 10 µl 0.5x concentration iRT standards and the samples are ready for LC-MS analysis. To build the spectral library, 20 µg from each sample was pooled. The pooled sample was desalted using a Waters Sep-Pak C18 cartridge. The desalted pooled sample was off-line fractionated into 16 fractions using high pH reversed phase HPLC method on a Waters Xbridge C18 chromatographic column. Around 5 µg peptide from each fraction was transferred to a new tube and dried down in a SpeedVac and reconstituted in 25 µl 0.1% formic acid. Ten µl sample was mixed with 10 µl 0.5x concentration iRT standards and the samples are ready for LCMS analysis. The LC-MS system was a Bruker timsTOF pro2 mass spectrometry system interfaced with a Bruker NanoElute HPLC system. The HPLC column was a BurkerFifteen 15 cm x 75 µm id reversed phase capillary chromatography column. Four µL of the sample were injected and the peptides eluted from the column by an acetonitrile/0.1% formic acid gradient at a flow rate of 0.3 µL/min were introduced into the source of the mass spectrometer on-line. The microelectrospray ion source is operated at 1.5 kV. For spectral library generation, the digest was analyzed using a data dependent acquisition (DDA) method, the instrument acquires full scans followed by MS/MS scans of the most abundant ions from the full scans in successive instrument scans. For LC-MS analysis of the samples, a data independent acquisition (DIA) method was used. The instrument acquires full scans followed by MS/MS scans of 32 fixed variable mass windows along the whole LC gradient. The spectral library was generated using Pulsar that is integrated in Spectronaut software package searching the DDA LC-MS data from the 16 fractions of the pooled sample. The DIA data were analyzed using Spectronaut V16 to search against the spectral library and the mouse UniProtKB protein sequence database for the identification and quantification of proteins and peptides. False discovery rate of protein was set at 1%. The relative protein abundance across these samples was determined using a label free approach. Protein quantities were expressed as normalized intensities by Spectronaut V16. These are based on the sum of the (raw) intensities of the MS/MS product ions of their peptide precursor peaks that are normalized to the total peptide amount in each sample to ensure that profiles of the abundances across samples accurately reflects the relative amounts of the proteins in the protein samples. Analysis of proteomics data to generate

networks as well as pathway analysis was performed using Ingenuity Pathway Analysis (2023 version).

Flow cytometry

Matrigel domes containing organoids were harvested (gentle pipetting up and down using P1000 pipette) and transferred to a 15 mL conical tube containing 1X PBS and 5 mM EDTA (Invitrogen, 15575-038). The tube was inverted 30 times to break up the organoids from Matrigel and centrifuged at 300xg for 5 minutes. Supernatant was removed and pellets were resuspended in 5 mL 1X TrypLE Express Enzyme (ThermoFisher Scientific, 12604021) containing Rho/ROCK inhibitor Y-27632 (1:1000 concentration). Conical tubes containing organoids were incubated at 37℃ for 5 minutes followed by vigorous pipetting using P1000 pipette to dissociate spheroid clumps into single cells. Organoid wash buffer (7 mL, 2X washes) was added to the tubes and centrifugation (300xg, 5 minutes) was performed to obtain cell pellets. LIVE/DEAD™ Fixable Blue Dead Cell Stain (ThermosFisher Scientific, L23105) was performed prior to fixation step. For Ki67 staining (BioLegend Ki67 staining flow protocol), cells were fixed in ice cold 70% ethanol (1 hour) followed by 3X washes in cell staining buffer (BioLegend, 420201). Subsequently, 100 µl of fluorochrome-conjugated Ki67 antibody (BioLegend, 652410) prepared in cell staining buffer was added to cells and incubation was performed for 30 minutes in the dark on a rocker (room temperature). Cells were washed 2X using cell staining buffer and resuspended in the buffer (0.3 mL) for flow cytometric analysis. Flow cytometry to measure apoptotic cell death was performed according to manufacturer's instructions using the Apoptosis/Necrosis assay (Abcam, AB176749). Staurosporine (Tocris, 1285) was used as a positive control for apoptosis assay. Sample acquisition was performed using BD LSRFortessa™ Cell Analyzer. Analysis was performed on the FlowJo software (version 10.9.0). Gating has been shown in **Supplemental Fig. 5D and Supplemental Fig. 6C**.

Statistical analysis

Statistical power for *in vitro* experiments was calculated based on preliminary data for ZO-1 protein expression in n=3 animals acquired from high glucose (25 mM, average protein expression 1.833) treatments in comparison to normal glucose (5 mM, average protein expression=2.719). Based on $\alpha<0.05$, power analysis revealed the requirement of at least 4 animals/group for *in vitro* experiments. Statistical analyses for western blot, qRT-PCR, and flow cytometry assays were performed using GraphPad Prism software (version 10). Quantitative protein analysis between groups (proteomics data) was performed using Spectronaut V16. All

data is presented as Mean ± SEM. The number of animals utilized for experiments is listed under each figure legend and shown as an individual data point in the graphs. All *in vitro* experiments were performed in at least in triplicate. For data sets with multiple treatment groups, One-way ANOVA (Dunnett's multiple comparisons test or post-hoc Tukey) was used. P value less than 0.05 was considered significant.

Data Availability Statement

The original contributions presented in the study are included in the article and supplementary material. Further inquiries can be directed to the corresponding authors. Original raw proteomics data has been made available in supplementary data files.

Correspondence

Address correspondence to: Samreen Jatana, Lerner Research Institute, Cleveland Clinic, Cleveland, Ohio, USA. E-mail: jatanas@ccf.org. Carol de la Motte, Lerner Research Institute, Cleveland Clinic, Cleveland, Ohio, USA. E-mail: delamoc@ccf.org.

Acknowledgements

We are grateful to Judith Drazba and Gauravi Deshpande of the Lerner Research Institute Digital Imaging Microscopy Core, who aided with confocal microscopy. We also thank the members of the Lerner Research Institute Flow Cytometry Core for their input on panel design and help with data acquisition. All schematics were created in BioRender.

Authorship Contributions

S.J. conceptualized the study, designed, and performed experiments, analyzed, and interpreted data, wrote and edited the manuscript, acquired funding. A.A. conceptualized the study, designed, and performed experiments, analyzed, and interpreted data, edited the manuscript. G.A.W. and A.K.P. conceptualized, designed, and performed experiments, and reviewed the manuscript. M.B.N. performed experiments and reviewed the manuscript. J.L.S. designed, and performed experiments, and reviewed the manuscript. A.M.M. analyzed data. B.W. performed experiments, analyzed, and interpreted data. L.E.N and C.dl.M. conceptualized the study, supported the design of experiments, supported the analyses and interpretation of data, wrote, and edited the manuscript, and acquired funding.

Conflict of Interest

The authors disclose no conflicts.

Funding

This work was supported by National Institutes of Health (NIH) grant R01AA023764 and Department of Defense (DOD) grant PR190724/ W81XWH2010235 to LEN and CdlM. This study was also funded by the Crohn's and Colitis Foundation Research Fellowship Award (Award# 662997) to SJ. This work utilized the Leica SP8 confocal microscope that was purchased with funding from the NIH Shared Instrumentation Grant 1S10OD019972-01. The Bruker timsTof Pro2

instrument used for proteomics analysis was purchased via an NIH Shared Instrument Grant, S10 OD030398.

FIGURES

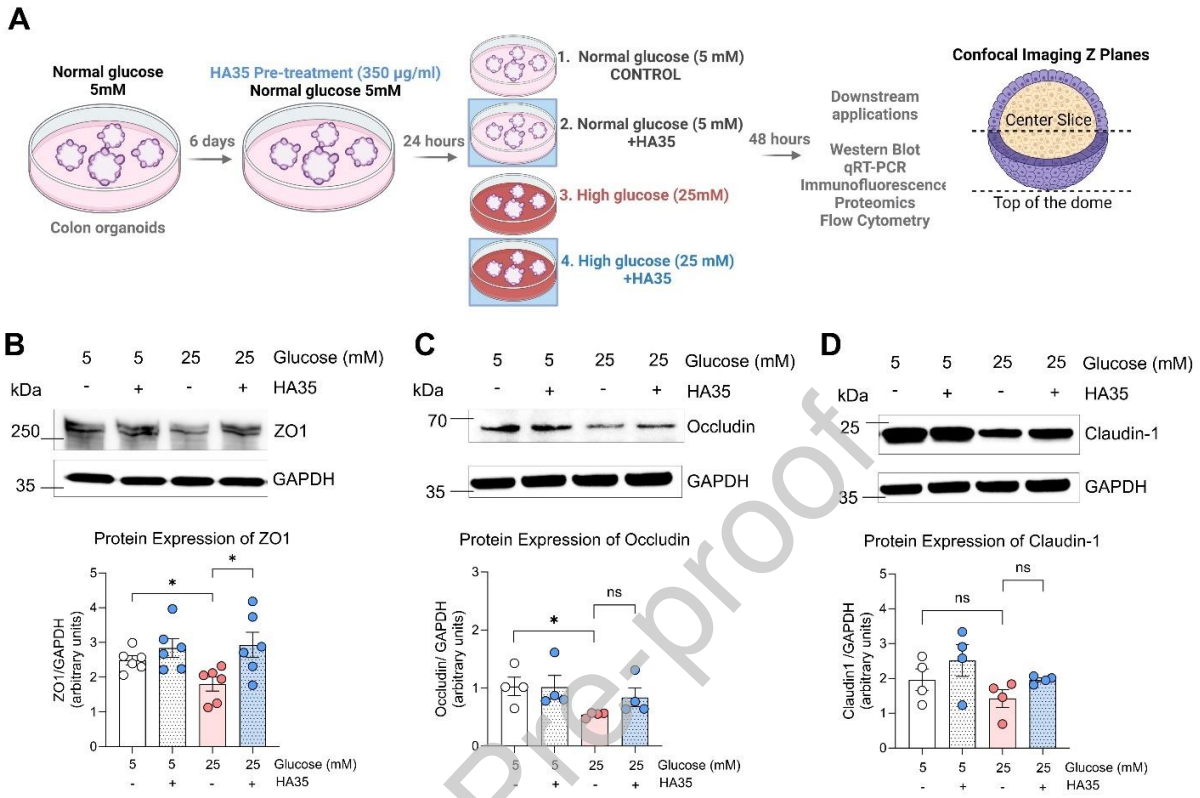

Fig. 1. HA35 protects against the effects of hyperglycemia on tight junction protein expression. (A) Schematic showing *in vitro* set up for organoid assays. Murine distal colon organoids were grown and expanded in media containing normal glucose (5 mM) for 6 days. Prior to addition of high glucose (25 mM), organoids were pre-treated with HA35 (350 µg/ml) for 24h. Organoids were collected for downstream assays 48h after addition of high glucose (25 mM) except for time course studies. Confocal images were taken either at the center of the dome (center slice) or the top of the organoid domes (B) Western blots and bar plots showing the quantification of ZO-1, occludin, and claudin-1 proteins in colonic organoids across four treatment groups (48h post-treatment). N=4-6 wild-type (WT) mouse organoids. Results are shown as Mean ± SEM. *p<0.05, one-way ANOVA in comparison to 5 mM control group and 25 mM high glucose group (Dunnett's multiple comparison test).

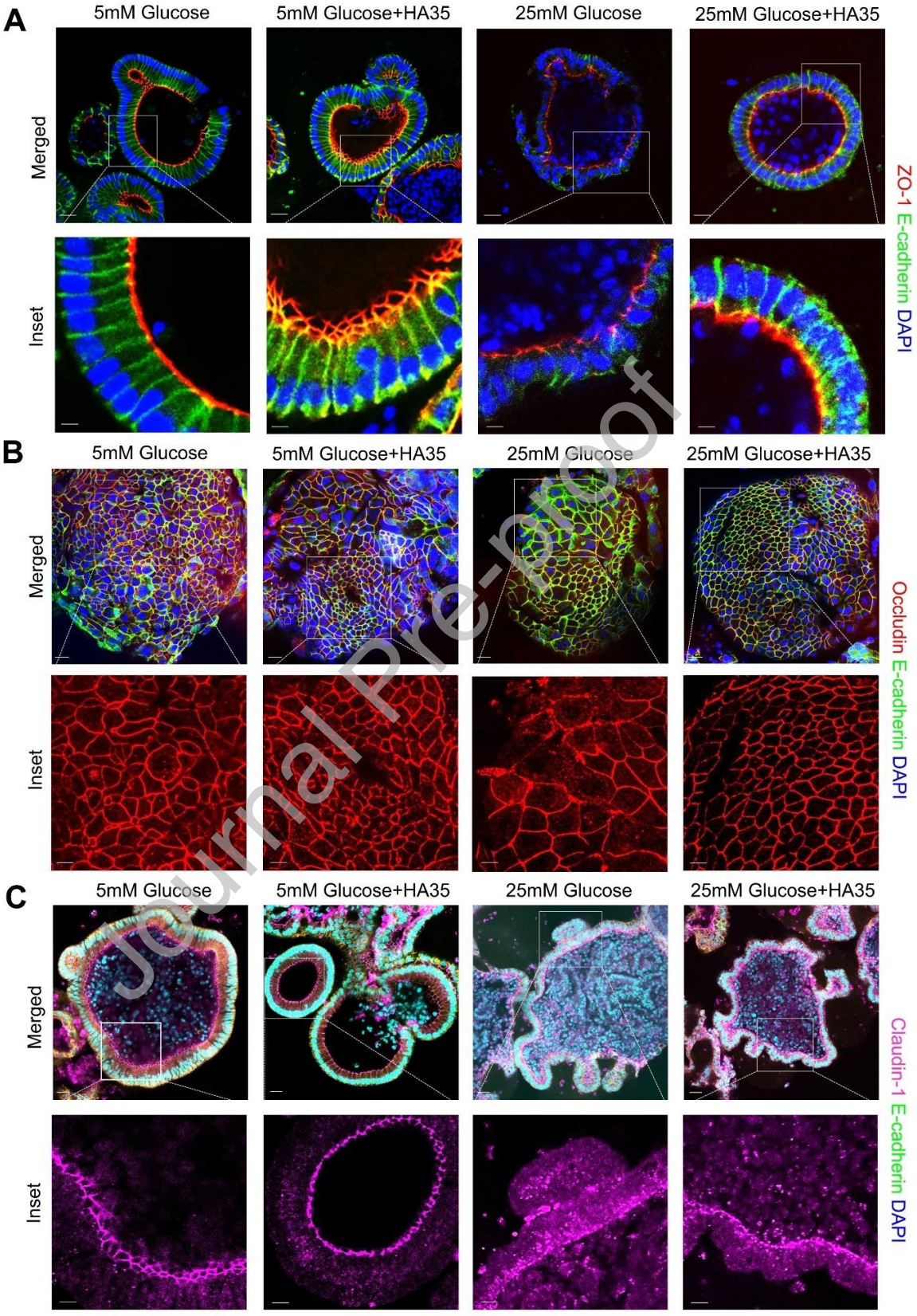

Fig. 2. HA35 pre-treatment maintains spatial distribution of ZO-1 and occludin under high glucose conditions. (A) Representative immunofluorescence (IF) images showing ZO-1 (red) and E-cadherin (green) staining in mouse colon organoids. Bottom panel: magnification of white boxes in top panel (inset). Images acquired at the center slice of spheroid dome. (B) Representative IF images showing occludin (red) and E-cadherin (green) staining in mouse colon organoids. Bottom panel: magnification of white boxes in top panel (inset). Images acquired at the top of the spheroid dome. (C) Representative IF images showing claudin-1 (magenta) and E-cadherin (yellow) in mouse colon organoids. Bottom panel: magnification of white boxes in top panel (inset). Images acquired at the center slice of spheroid dome. DAPI marks nuclei in blue. All images were acquired using confocal microscopy. Top panels were acquired using 40X oil objective and insets (bottom panels) using 63X oil objective. Representative images from N=3 WT mouse organoids, 48h post-treatment. Scale bar=20 µm (Inset=5 µm).

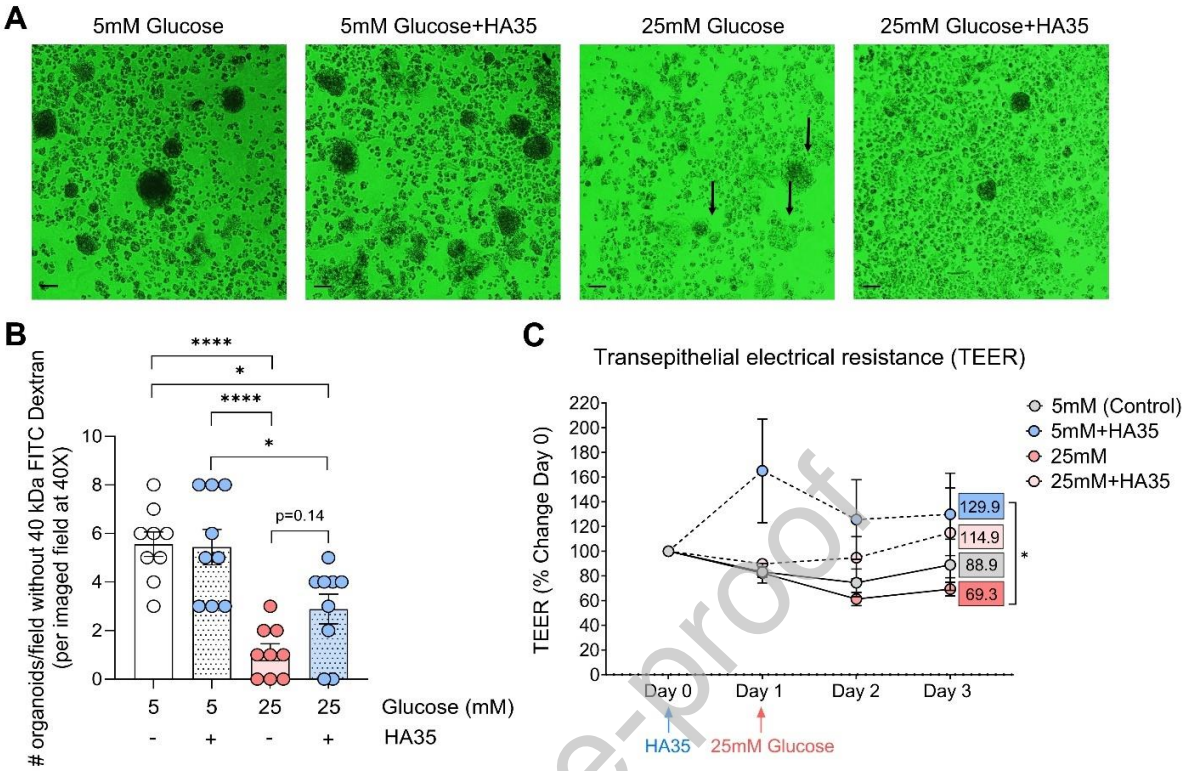

Fig. 3. HA35 protects functional barrier integrity under hyperglycemic stress. (A) Representative images from mouse colon "flipped apical surface out" organoids pre-treated with HA35 followed by addition of high glucose (25 mM). 40 kDa FITC-dextran was added to visualize outside-in (apical to basolateral) flux to measure barrier function. Organoids with dark centers indicative of reduced FITC-dextran transit. Alternatively, organoid centers that were fluorescent green were indicative of impaired barrier or increased FITC transit (black arrows). Images acquired using confocal microscopy (40X oil objective). Scale bar=20 μm. (B) Bar plot showing the number of organoids per field containing dark centers. N=3 WT mouse organoids, n=3 images acquired per treatment group, 48h post-treatment with high glucose (25 mM) and 10 minutes post-treatment with 40 kDa FITC-dextran. *p<0.05, ****p<0.0001, one-way ANOVA (inter group analysis, post-hoc Tukey). (C) Transepithelial electrical resistance (TEER) measured in monolayers across the four treatment groups over a period of 4 days. TEER values were normalized to Day 0 measurements (start of the experiment). *p<0.05, unpaired t-Test with Welch's correction. Monolayers were grown from N=5 WT mouse organoids.

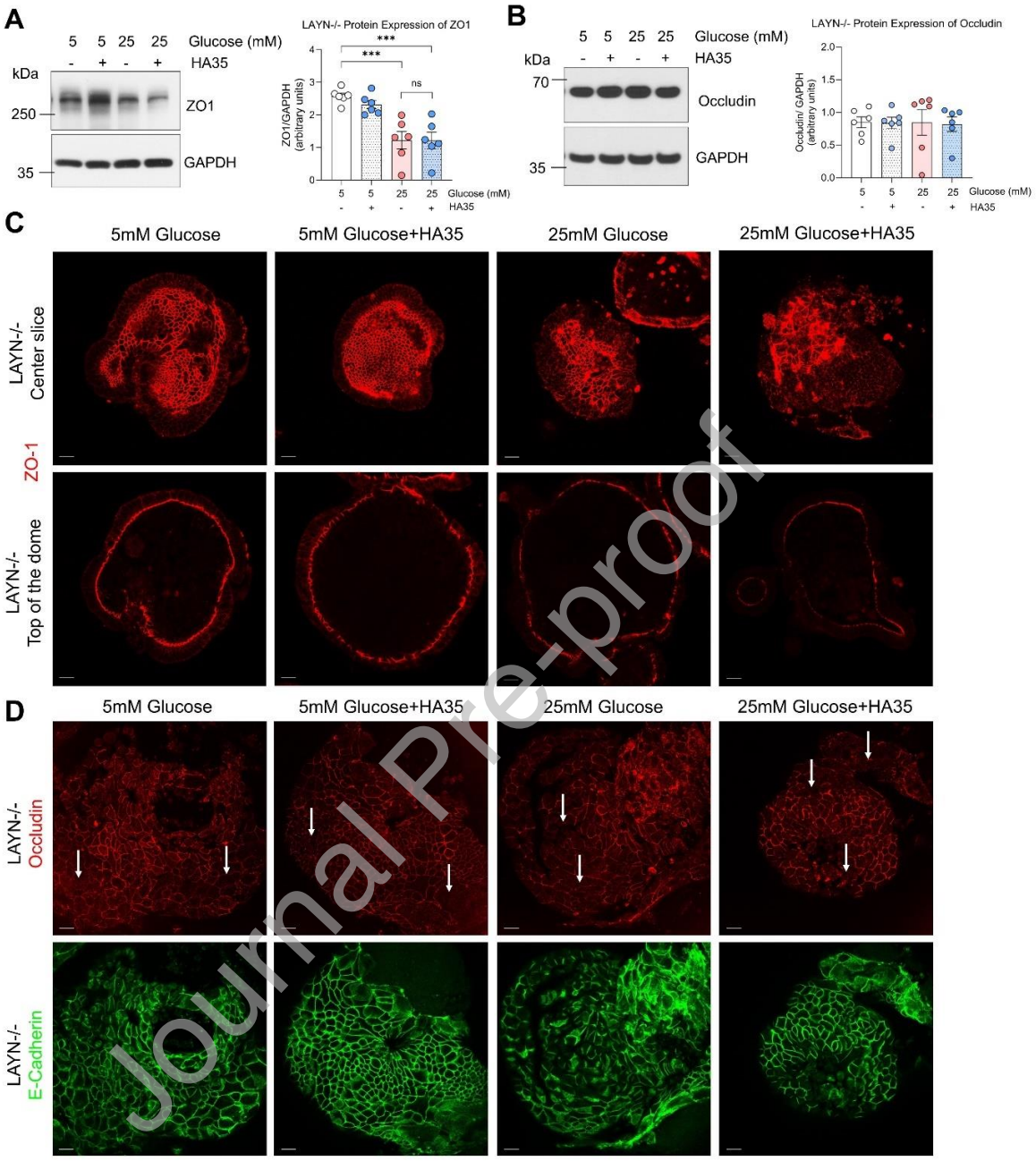

Fig. 4. HA receptor, layilin, is involved in the maintenance of barrier integrity under hyperglycemic stress. (A) Representative western blot and quantification (densitometry) of protein expression of ZO-1 in LAYN-/- organoid lysates across the four treatment groups. N=6 LAYN-/- mouse organoids, 48h post-treatment, ***p<0.001, one-way ANOVA (in comparison to 5 mM control and 25 mM high glucose, Dunnett's multiple comparison test). (B) Representative western blot and quantification (densitometry) of protein expression of occludin in LAYN-/-

organoid lysates across the four treatment groups. N=6 LAYN-/- mouse organoids, 48h post-treatment. (C) Representative IF images showing ZO-1 (red) staining in LAYN-/- organoids across the four treatment groups. Top panel shows images acquired at the top of organoid domes and bottom panels show images acquired at the center slice. (D) Representative IF images showing occludin (red) and E-cadherin (green) staining in LAYN-/- mouse organoids across the four treatment groups. Images were obtained at the top of the organoid domes. All IF images were acquired using a confocal microscope (40X oil objective), representative N=3 LAYN-/- mouse organoids, 48h post-treatment. Scale bar=20 μm.

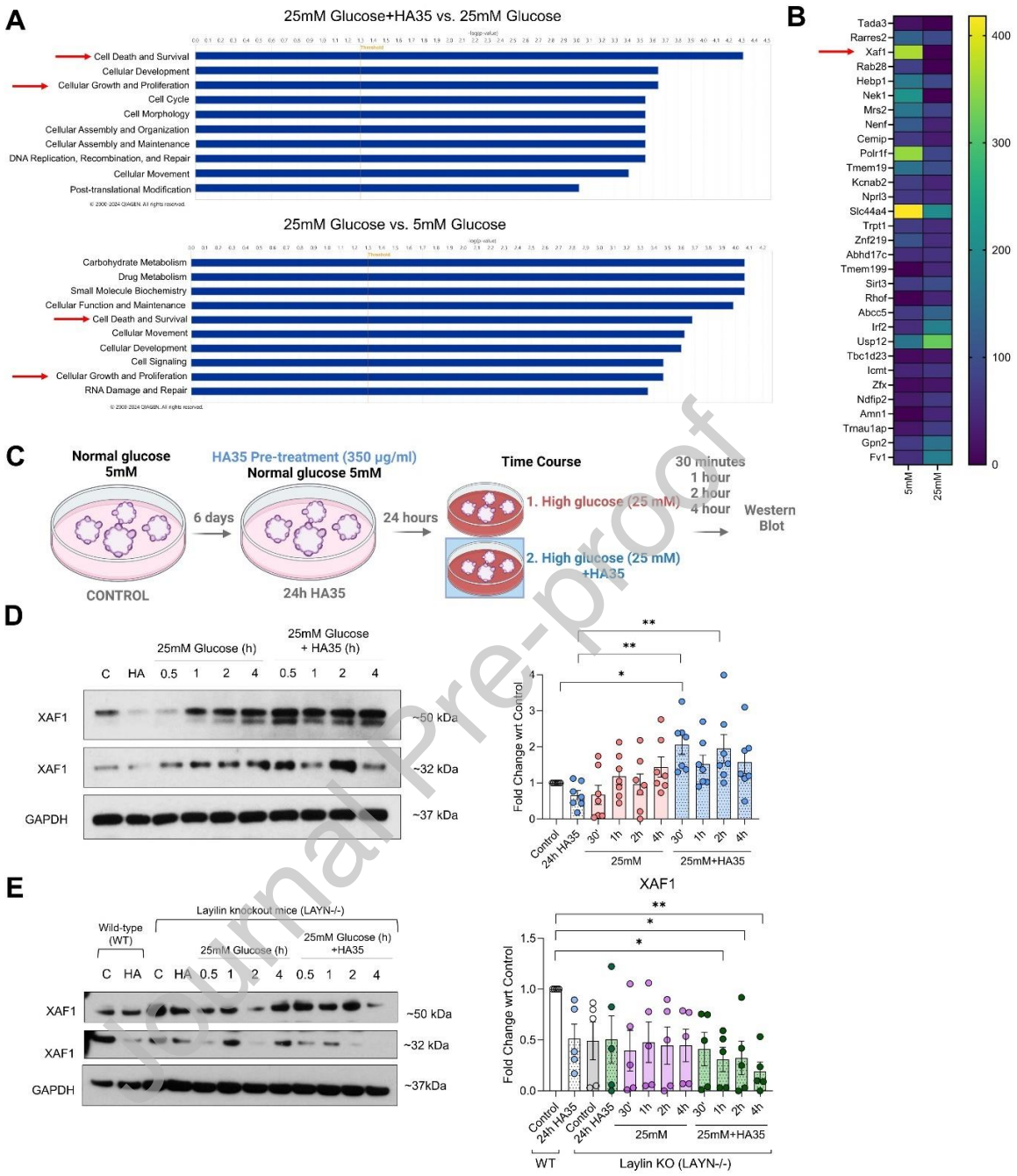

Fig. 5. HA35 regulates cell death and survival under high glucose stress. (A) Pathway analysis using IPA software to identify top cellular pathways upregulated in 25 mM glucose+HA35 vs. 25 mM glucose (top) and 25 mM glucose vs. 5 mM glucose treatment groups (bottom). Threshold set at 1.3 -log (p-value). N=4 WT mouse organoids, 48h post-treatment. (B) Heatmaps generated from proteomics data showing changes (up- and downregulated) in proteins that were

significantly up- or downregulated 48h post-treatment in high glucose (25 mM) treatment vs. normal glucose controls (5 mM), $p<0.05$. (C) Schematic showing *in vitro* organoid set up for western blot time course experiments. Samples were collected 30 minutes, 1h, 2h and 4h post-treatment. (D) Representative western blot and quantification (densitometry) of protein expression of Xaf1 in organoid lysates across the four treatment groups. Xaf1 has two separate bands detected at ~50 kDa and ~32 kDa size. N=6 WT mouse organoids utilized for western blotting. *$p<0.05$, **$p<0.01$, one-way ANOVA (analyses performed in comparison to 5 mM control as well as 24h HA35 treatment control, Dunnett's multiple comparison test). (E) Representative western blots and quantification (densitometry) of protein expression of Xaf1 in LAYN-/- organoid lysates across four treatment groups. First two lanes in the gel are WT organoids grown in 5 mM media control (C) and WT organoids treated with HA35 for 24h. N=5 LAYN-/- mouse organoids utilized for western blotting, *$p<0.05$ in comparison to WT control (C), one-way ANOVA (Dunnett's multiple comparison test).

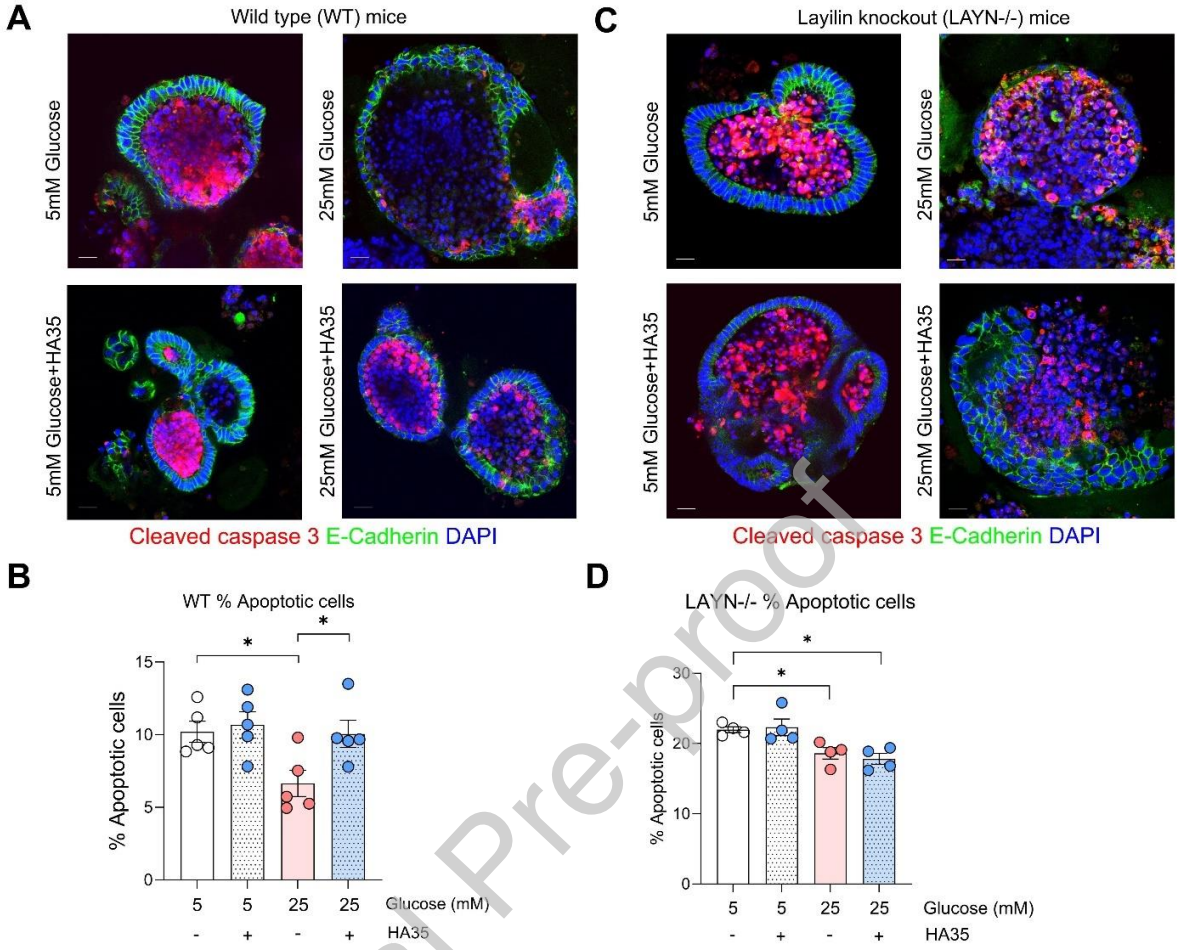

Fig. 6. HA35 counteracts the effect of hyperglycemic stress apoptotic cell death. (A) Representative IF images showing cleaved caspase-3 (red) and E-cadherin (green) staining in WT organoids. DAPI are marked in blue. Representative images from N=3 WT mouse organoids. Scale bar=20 µm. (B) Bar plot showing percentage of apoptotic cells measured by flow cytometry. N=5 WT mouse organoids. *p<0.05, one-way ANOVA, inter-group analysis performed in comparison to 5 mM control and 25 mM high glucose treatment (Dunnett's multiple comparison test). (C) Representative IF images showing cleaved caspase-3 (red) and E-cadherin (green) staining in LAYN-/- organoids. DAPI are marked in blue. Representative images from N=3 LAYN-/- mouse organoids. Scale bar=20 µm. (D) Bar plot showing percentage of apoptotic cells measured by flow cytometry. N=4 LAYN-/- mouse organoids. *p<0.05, one-way ANOVA, inter-group analysis performed in comparison to control (Dunnett's multiple comparison test).

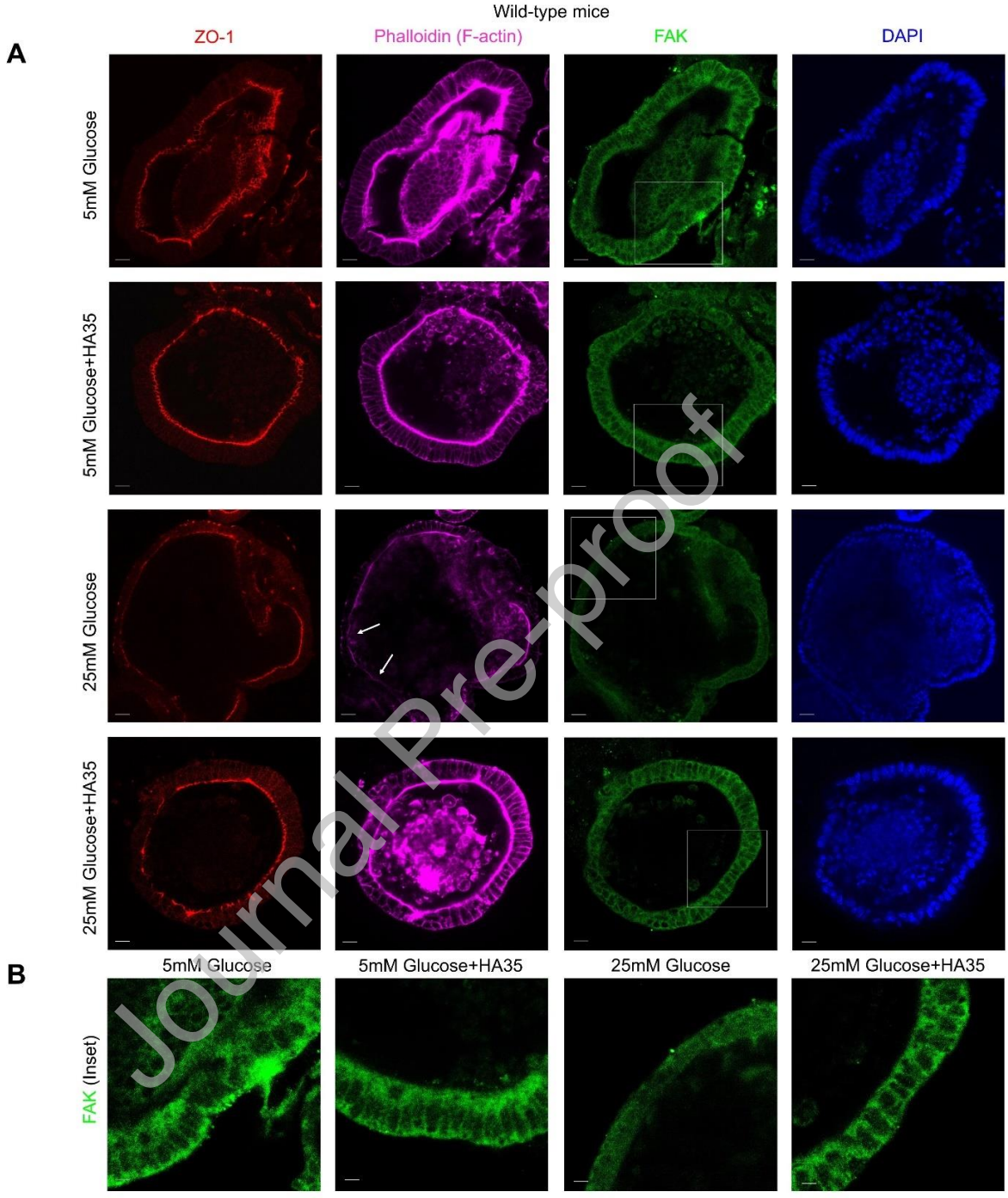

Fig. 7. HA35 maintains spatial distribution of F-actin and focal adhesion kinase (FAK) under high glucose conditions. (A) Representative IF images showing ZO-1 (red), F-actin (phalloidin, magenta), and focal adhesion kinase (FAK, green) staining in WT organoids. DAPI are marked in blue. Representative images from N=3 WT mouse organoids. Scale bar=20 μm. (B) FAK staining

(green) inset from regions highlighted in white box (panel A). Scale bar=5 μm. All images are acquired at the center slice of the organoid dome.

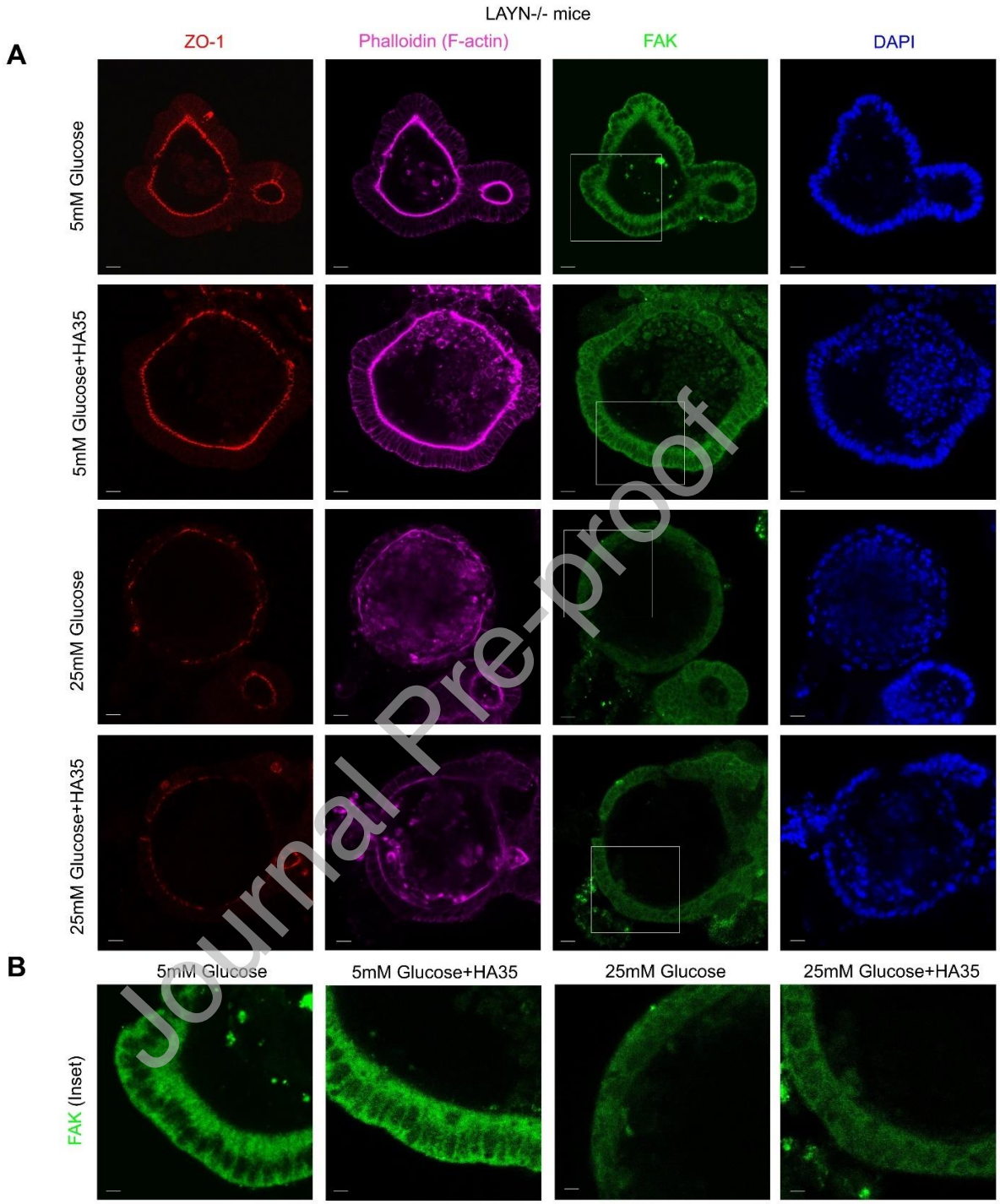

Fig. 8. HA35 maintains spatial distribution of F-actin and focal adhesion kinase (FAK) under high glucose conditions via layilin. (A) Representative IF images showing ZO-1 (red), F-actin (phalloidin, magenta), and focal adhesion kinase (FAK, green) staining in LAYN-/- organoids. DAPI are marked in blue. Representative images from N=3 LAYN-/- mouse organoids. Scale

bar=20 μm. (B) FAK staining (green) inset from regions highlighted in white box (panel A). Scale bar=5 μm. All images are acquired at the center slice of the organoid dome.

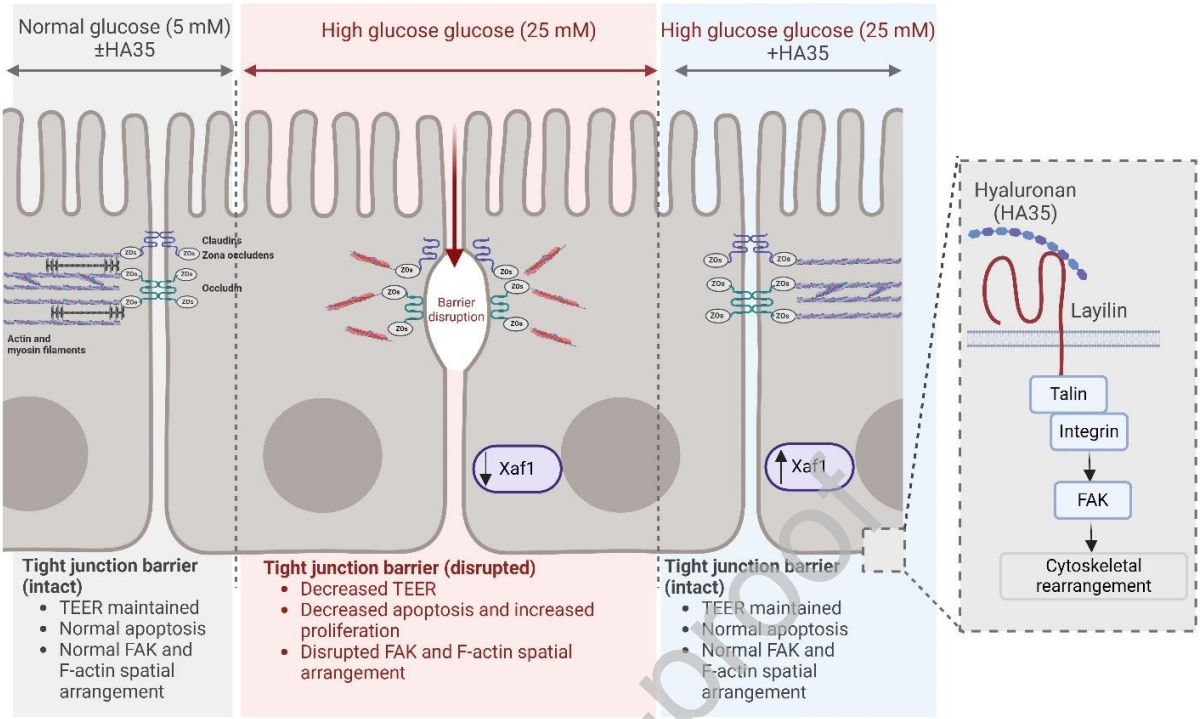

Fig. 9. Schematic summarizing findings from the study. In this study, we showed that hyperglycemic stress increases protein loss (ZO-1) and spatial distribution (ZO-1, occludin) of key intestinal barrier proteins in a mouse intestinal organoid model. Small molecular weight hyaluronan (35 kDa), HA35, plays a protective effect on barrier function under high glucose conditions via layilin. HA35 regulates apoptotic cell death in organoids grown under hyperglycemic stress by modulating the levels of Xaf1 protein. HA35 maintains the spatial arrangement of FAK and F-actin under hyperglycemic stress. The effects of HA35 on the intestinal barrier function are likely regulated by its receptor layilin via the layilin-integrin-FAK axis.

References

[1] M.W. Schleh, H.L. Caslin, J.N. Garcia, M. Mashayekhi, G. Srivastava, A.B. Bradley, A.H. Hasty, Metaflammation in obesity and its therapeutic targeting, Sci Transl Med 15(723) (2023) eadf9382.

[2] G.S. Hotamisligil, Inflammation, metaflammation and immunometabolic disorders, Nature 542(7640) (2017) 177-185.

[3] N.C.D.R.F. Collaboration, Worldwide trends in underweight and obesity from 1990 to 2022: a pooled analysis of 3663 population-representative studies with 222 million children, adolescents, and adults, Lancet 403(10431) (2024) 1027-1050.

[4] C. Priest, P. Tontonoz, Inter-organ cross-talk in metabolic syndrome, Nat Metab 1(12) (2019) 1177-1188.

[5] B. Ma, X. Wang, H. Ren, Y. Li, H. Zhang, M. Yang, J. Li, High glucose promotes the progression of colorectal cancer by activating the BMP4 signaling and inhibited by glucagon-like peptide-1 receptor agonist, BMC Cancer 23(1) (2023) 594.

[6] C.Y. Lin, C.H. Lee, C.C. Huang, S.T. Lee, H.R. Guo, S.B. Su, Impact of high glucose on metastasis of colon cancer cells, World J Gastroenterol 21(7) (2015) 2047-57.

[7] A. Vulcan, J. Manjer, B. Ohlsson, High blood glucose levels are associated with higher risk of colon cancer in men: a cohort study, BMC Cancer 17(1) (2017) 842.

[8] J. Xu, Y. Ye, H. Wu, P. Duerksen-Hughes, H. Zhang, P. Li, J. Huang, J. Yang, Y. Wu, D. Xia, Association between markers of glucose metabolism and risk of colorectal cancer, BMJ Open 6(6) (2016) e011430.

[9] A. De Filippis, H. Ullah, A. Baldi, M. Dacrema, C. Esposito, E.U. Garzarella, C. Santarcangelo, A. Tantipongpiradet, M. Daglia, Gastrointestinal Disorders and Metabolic Syndrome: Dysbiosis as a Key Link and Common Bioactive Dietary Components Useful for their Treatment, Int J Mol Sci 21(14) (2020).

[10] M.M. Sang, Z.L. Sun, T.Z. Wu, Inflammatory bowel disease and diabetes: Is there a link between them?, World J Diabetes 13(2) (2022) 126-128.

[11] E.A. Kang, K. Han, J. Chun, H. Soh, S. Park, J.P. Im, J.S. Kim, Increased Risk of Diabetes in Inflammatory Bowel Disease Patients: A Nationwide Population-based Study in Korea, J Clin Med 8(3) (2019).

[12] C.K. Hyun, Molecular and Pathophysiological Links between Metabolic Disorders and Inflammatory Bowel Diseases, Int J Mol Sci 22(17) (2021).

[13] T. Lawler, Z.L. Walts, M. Steinwandel, L. Lipworth, H.J. Murff, W. Zheng, S. Warren Andersen, Type 2 Diabetes and Colorectal Cancer Risk, JAMA Netw Open 6(11) (2023) e2343333.

[14] C. Zihni, C. Mills, K. Matter, M.S. Balda, Tight junctions: from simple barriers to multifunctional molecular gates, Nat Rev Mol Cell Biol 17(9) (2016) 564-80.

[15] S. Lechuga, M.B. Braga-Neto, N.G. Naydenov, F. Rieder, A.I. Ivanov, Understanding disruption of the gut barrier during inflammation: Should we abandon traditional epithelial cell lines and switch to intestinal organoids?, Front Immunol 14 (2023) 1108289.

[16] N. Di Tommaso, A. Gasbarrini, F.R. Ponziani, Intestinal Barrier in Human Health and Disease, Int J Environ Res Public Health 18(23) (2021).

[17] S. Riedel, C. Pheiffer, R. Johnson, J. Louw, C.J.F. Muller, Intestinal Barrier Function and Immune Homeostasis Are Missing Links in Obesity and Type 2 Diabetes Development, Front Endocrinol (Lausanne) 12 (2021) 833544.

[18] L. Shen, L. Ao, H. Xu, J. Shi, D. You, X. Yu, W. Xu, J. Sun, F. Wang, Poor short-term glycemic control in patients with type 2 diabetes impairs the intestinal mucosal barrier: a prospective, single-center, observational study, BMC Endocr Disord 19(1) (2019) 29.

[19] Y.F. Wang, F.M. Liang, M. Liu, L.C. Ding, J.J. Hui, H.Y. Xu, L.J. Liu, Is compromised intestinal barrier integrity responsible for the poor prognosis in critically ill patients with pre-existing hyperglycemia?, Diabetol Metab Syndr 14(1) (2022) 172.

[20] J.H. Yuan, Q.S. Xie, G.C. Chen, C.L. Huang, T. Yu, Q.K. Chen, J.Y. Li, Impaired intestinal barrier function in type 2 diabetic patients measured by serum LPS, Zonulin, and IFABP, J Diabetes Complications 35(2) (2021) 107766.

[21] C.A. Thaiss, M. Levy, I. Grosheva, D. Zheng, E. Soffer, E. Blacher, S. Braverman, A.C. Tengeler, O. Barak, M. Elazar, R. Ben-Zeev, D. Lehavi-Regev, M.N. Katz, M. Pevsner-Fischer, A. Gertler, Z. Halpern, A. Harmelin, S. Aamar, P. Serradas, A. Grosfeld, H. Shapiro, B. Geiger, E. Elinav, Hyperglycemia drives intestinal barrier dysfunction and risk for enteric infection, Science 359(6382) (2018) 1376-1383.

[22] N. Dubois, J. Munoz-Garcia, D. Heymann, A. Renodon-Corniere, High glucose exposure drives intestinal barrier dysfunction by altering its morphological, structural and functional properties, Biochem Pharmacol 216 (2023) 115765.

[23] Y. Kim, C.A. de la Motte, The Role of Hyaluronan Treatment in Intestinal Innate Host Defense, Front Immunol 11 (2020) 569.

[24] A.C. Petrey, C.A. de la Motte, Hyaluronan, a crucial regulator of inflammation, Front Immunol 5 (2014) 101.

[25] S.P. Kessler, D.R. Obery, K.P. Nickerson, A.C. Petrey, C. McDonald, C.A. de la Motte, Multifunctional Role of 35 Kilodalton Hyaluronan in Promoting Defense of the Intestinal Epithelium, J Histochem Cytochem 66(4) (2018) 273-287.

[26] Y. Kim, S.P. Kessler, D.R. Obery, C.R. Homer, C. McDonald, C.A. de la Motte, Hyaluronan 35kDa treatment protects mice from Citrobacter rodentium infection and induces epithelial tight junction protein ZO-1 in vivo, Matrix Biol 62 (2017) 28-39.

[27] Y. Kim, G.A. West, G. Ray, S.P. Kessler, A.C. Petrey, C. Fiocchi, C. McDonald, M.S. Longworth, L.E. Nagy, C.A. de la Motte, Layilin is critical for mediating hyaluronan 35kDa-induced intestinal epithelial tight junction protein ZO-1 in vitro and in vivo, Matrix Biol 66 (2018) 93-109.

[28] C.A. de la Motte, Hyaluronan in intestinal homeostasis and inflammation: implications for fibrosis, Am J Physiol Gastrointest Liver Physiol 301(6) (2011) G945-9.

[29] A. Gunasekaran, J. Eckert, K. Burge, W. Zheng, Z. Yu, S. Kessler, C. de la Motte, H. Chaaban, Hyaluronan 35 kDa enhances epithelial barrier function and protects against the development of murine necrotizing enterocolitis, Pediatr Res 87(7) (2020) 1177-1184.

[30] D.R. Hill, H.K. Rho, S.P. Kessler, R. Amin, C.R. Homer, C. McDonald, M.K. Cowman, C.A. de la Motte, Human milk hyaluronan enhances innate defense of the intestinal epithelium, J Biol Chem 288(40) (2013) 29090-104.

[31] D.A. Bellos, D. Sharma, M.R. McMullen, J. Wat, P. Saikia, C.A. de la Motte, L.E. Nagy, Specifically Sized Hyaluronan (35 kDa) Prevents Ethanol-Induced Disruption of Epithelial Tight Junctions Through a layilin-Dependent Mechanism in Caco-2 Cells, Alcohol Clin Exp Res 43(9) (2019) 1848-1858.

[32] S. Ray, E. Huang, G.A. West, M. Mrdjen, M.R. McMullen, C. de la Motte, L.E. Nagy, 35kDa hyaluronan ameliorates ethanol driven loss of anti-microbial defense and intestinal barrier integrity in a TLR4-dependent manner, Matrix Biol 115 (2023) 71-80.

[33] A. Bellar, S.P. Kessler, D.R. Obery, N. Sangwan, N. Welch, L.E. Nagy, S. Dasarathy, C. de la Motte, Safety of Hyaluronan 35 in Healthy Human Subjects: A Pilot Study, Nutrients 11(5) (2019).

[34] H. Miyoshi, T.S. Stappenbeck, In vitro expansion and genetic modification of gastrointestinal stem cells in spheroid culture, Nat Protoc 8(12) (2013) 2471-82.

[35] J.Y. Co, M. Margalef-Catala, D.M. Monack, M.R. Amieva, Controlling the polarity of human gastrointestinal organoids to investigate epithelial biology and infectious diseases, Nat Protoc 16(11) (2021) 5171-5192.

[36] S.I. Jeong, J.W. Kim, K.P. Ko, B.K. Ryu, M.G. Lee, H.J. Kim, S.G. Chi, XAF1 forms a positive feedback loop with IRF-1 to drive apoptotic stress response and suppress tumorigenesis, Cell Death Dis 9(8) (2018) 806.

[37] W.T. Kuo, M.A. Odenwald, J.R. Turner, L. Zuo, Tight junction proteins occludin and ZO-1 as regulators of epithelial proliferation and survival, Ann N Y Acad Sci 1514(1) (2022) 21-33.

[38] A.P. Soler, R.D. Miller, K.V. Laughlin, N.Z. Carp, D.M. Klurfeld, J.M. Mullin, Increased tight junctional permeability is associated with the development of colon cancer, Carcinogenesis 20(8) (1999) 1425-31.

[39] A.A. Bhat, S. Uppada, I.W. Achkar, S. Hashem, S.K. Yadav, M. Shanmugakonar, H.A. Al-Naemi, M. Haris, S. Uddin, Tight Junction Proteins and Signaling Pathways in Cancer and Inflammation: A Functional Crosstalk, Front Physiol 9 (2018) 1942.

[40] J.E. Glasgow, J.R. Byrnes, S.D. Barbee, J.M. Moreau, M.D. Rosenblum, J.A. Wells, Identifying and antagonizing the interactions between layilin and glycosylated collagens, Cell Chem Biol 29(4) (2022) 597-604 e7.

[41] Y.A. Kadry, D.A. Calderwood, Chapter 22: Structural and signaling functions of integrins, Biochim Biophys Acta Biomembr 1862(5) (2020) 183206.

[42] D.A. Calderwood, I.D. Campbell, D.R. Critchley, Talins and kindlins: partners in integrin-mediated adhesion, Nat Rev Mol Cell Biol 14(8) (2013) 503-17.

[43] M.D. Bass, B.J. Smith, S.A. Prigent, D.R. Critchley, Talin contains three similar vinculin-binding sites predicted to form an amphipathic helix, Biochem J 341 (Pt 2)(Pt 2) (1999) 257-63.

[44] Y. Ma, S. Semba, R.I. Khan, H. Bochimoto, T. Watanabe, M. Fujiya, Y. Kohgo, Y. Liu, T. Taniguchi, Focal adhesion kinase regulates intestinal epithelial barrier function via redistribution of tight junction, Biochim Biophys Acta 1832(1) (2013) 151-9.

[45] A. Aliluev, S. Tritschler, M. Sterr, L. Oppenlander, J. Hinterdobler, T. Greisle, M. Irmler, J. Beckers, N. Sun, A. Walch, K. Stemmer, A. Kindt, J. Krumsiek, M.H. Tschop, M.D. Luecken, F.J. Theis, H. Lickert, A. Bottcher, Diet-induced alteration of intestinal stem cell function underlies obesity and prediabetes in mice, Nat Metab 3(9) (2021) 1202-1216.

[46] B.D. Manning, A. Toker, AKT/PKB Signaling: Navigating the Network, Cell 169(3) (2017) 381-405.

[47] M. Li, S. Wang, S. Wang, L. Zhang, D. Wu, R. Yang, A. Ji, Y. Li, J. Wang, Occludin downregulation in high glucose is regulated by SSTR(2) via the VEGF/NRP1/Akt signaling pathway in RF/6A cells, Exp Ther Med 14(2) (2017) 1732-1738.

[48] L. Gonzalez-Mariscal, R. Tapia, D. Chamorro, Crosstalk of tight junction components with signaling pathways, Biochim Biophys Acta 1778(3) (2008) 729-56.

[49] X. Cong, W. Kong, Endothelial tight junctions and their regulatory signaling pathways in vascular homeostasis and disease, Cell Signal 66 (2020) 109485.

[50] Y. Peng, Y. Wang, C. Zhou, W. Mei, C. Zeng, PI3K/Akt/mTOR Pathway and Its Role in Cancer Therapeutics: Are We Making Headway?, Front Oncol 12 (2022) 819128.

[51] X. Zhang, M. Monnoye, M. Mariadassou, F. Beguet-Crespel, N. Lapaque, C. Heberden, V. Douard, Glucose but Not Fructose Alters the Intestinal Paracellular Permeability in Association With Gut Inflammation and Dysbiosis in Mice, Front Immunol 12 (2021) 742584.

[52] J. Wang, Q. Gu, M. Li, W. Zhang, M. Yang, B. Zou, S. Chan, L. Qiao, B. Jiang, S. Tu, J. Ma, I.F. Hung, H.Y. Lan, B.C. Wong, Identification of XAF1 as a novel cell cycle regulator through modulating G(2)/M checkpoint and interaction with checkpoint kinase 1 in gastrointestinal cancer, Carcinogenesis 30(9) (2009) 1507-16.

[53] R. Singh, A. Letai, K. Sarosiek, Regulation of apoptosis in health and disease: the balancing act of BCL-2 family proteins, Nat Rev Mol Cell Biol 20(3) (2019) 175-193.

[54] M. Chen, K. Wang, Y. Han, S. Yan, H. Yuan, Q. Liu, L. Li, N. Li, H. Zhu, D. Lu, K. Wang, F. Liu, D. Luo, Y. Zhang, J. Jiang, D. Li, L. Zhang, H. Ji, H. Zhou, Y. Chen, J. Qin, D. Gao, Identification of XAF1 as an endogenous AKT inhibitor, Cell Rep 42(7) (2023) 112690.

[55] W.T. Kuo, L. Zuo, M.A. Odenwald, S. Madha, G. Singh, C.B. Gurniak, C. Abraham, J.R. Turner, The Tight Junction Protein ZO-1 Is Dispensable for Barrier Function but Critical for Effective Mucosal Repair, Gastroenterology 161(6) (2021) 1924-1939.

[56] M.S. Balda, M.D. Garrett, K. Matter, The ZO-1-associated Y-box factor ZONAB regulates epithelial cell proliferation and cell density, J Cell Biol 160(3) (2003) 423-32.

[57] J. Xu, S.B. Lim, M.Y. Ng, S.M. Ali, J.P. Kausalya, V. Limviphuvadh, S. Maurer-Stroh, W. Hunziker, ZO-1 regulates Erk, Smad1/5/8, Smad2, and RhoA activities to modulate self-renewal and differentiation of mouse embryonic stem cells, Stem Cells 30(9) (2012) 1885-900.

[58] W.T. Kuo, L. Shen, L. Zuo, N. Shashikanth, M. Ong, L. Wu, J. Zha, K.L. Edelblum, Y. Wang, Y. Wang, S.P. Nilsen, J.R. Turner, Inflammation-induced Occludin Downregulation Limits Epithelial Apoptosis by Suppressing Caspase-3 Expression, Gastroenterology 157(5) (2019) 1323-1337.

[59] A.M. Carvalho, R.L. Reis, I. Pashkuleva, Hyaluronan Receptors as Mediators and Modulators of the Tumor Microenvironment, Adv Healthc Mater 12(5) (2023) e2202118.

[60] K.A. Owen, M.Y. Abshire, R.W. Tilghman, J.E. Casanova, A.H. Bouton, FAK regulates intestinal epithelial cell survival and proliferation during mucosal wound healing, PLoS One 6(8) (2011) e23123.

[61] K.L. VanDussen, N.M. Sonnek, T.S. Stappenbeck, L-WRN conditioned medium for gastrointestinal epithelial stem cell culture shows replicable batch-to-batch activity levels across multiple research teams, Stem Cell Res 37 (2019) 101430.

[62] T. Sato, R.G. Vries, H.J. Snippert, M. van de Wetering, N. Barker, D.E. Stange, J.H. van Es, A. Abo, P. Kujala, P.J. Peters, H. Clevers, Single Lgr5 stem cells build crypt-villus structures in vitro without a mesenchymal niche, Nature 459(7244) (2009) 262-5.